CHARACTERIZATION OF AIRBORNE BRAKE WEAR DEBRIS

FINAL REPORT

Submitted to

Association of Bay Area Governments
c/o Marcia Brockbank
San Francisco Estuary Project
1515 Clay Street, Suite 1400
Oakland, CA 94612

by

Ashley Haselden, Christos Christoforou, and Mark Schlautman
School of the Environment
Clemson University
342 Computer Court, Anderson, SC 29625

Original Submission Date: January 2005
Amended and Revised: January 2006

Explanation of Revisions

The original report entitled *Characterization of Airborne Brake Wear Debris* was submitted for review in 2004 and printed in January 2005. After the report was printed, a request was made to amend it to include airborne particle size distribution (PSD) information for the hypothetical composite (i.e., representative) brake pad wear debris (BPWD) sample so that it could be used as direct input into an air deposition model being used in a companion study to predict the atmospheric transport of copper from BPWD.

Changes from the original January 2005 final report are:

- Addition of Appendix E, which presents the requested PSD information for the representative BPWD sample as required for input to the air deposition model.
- Addition of Section 6c, which presents the calculation and uncertainty in the overall mass mean diameter of the representative BPWD sample.
- Addition of text at the end of Sections 7b and 7d which provides the mass mean diameters and associated uncertainties calculated from the measured Cu and Fe contents, respectively, of the representative BPWD sample.
- Use of more precise language to clearly distinguish between the terms *mass mean diameter* and *mass median diameter* that are utilized throughout the report.
- Removal of typographic and minor calculation errors that were found in the original report.

Acknowledgments

We gratefully acknowledge the laboratory assistance provided by Dr. Jin Hur at Clemson University. We also wish to thank the engineers and technicians at Link Testing Laboratories, Inc., particular Jason Sladich who assisted with the dynamometer setup during the aerodynamic particle size measurements. Professor James J. Schauer at the University of Wisconsin-Madison generously provided the MOUDI samplers for our use in this study. Industry members of the Brake Pad Partnership Steering Committee (Pat Thesier, Sumitomo Electric Automotive, Inc.; Dr. Tim Merkel, representing friction material manufacturers; Roger Dabish, TMD Friction, Inc.; Chris Shepley, Brake Parts Inc.; Dr. Mark Phipps, Federal Mogul Corporation) were instrumental in identifying and obtaining the brake pad materials used in this study, which were generously provided by the Brake Manufacturers Council Product Environmental Committee.

Other Brake Pad Partnership Steering Committee members (Dr. Kelly Moran, representing the Bay Area Stormwater Management Agencies Association; Jim Pendergast, U.S. Environmental Protection Agency; Michael Endicott, representing the Sierra Club) also provided immeasurable support. The Brake Pad Partnership (http://www.suscon.org/brakepad/index.asp) is a multistakeholder effort to understand the impacts on the environment that may arise from brake pad wear debris generated from passenger vehicles. Through the Partnership, manufacturers, regulators, stormwater management agencies, and environmentalists are working together to develop a process to evaluate such potential impacts, using copper in brake pads and water quality in the South San Francisco Bay as a case study.

Additional thanks go to Dr. Sarah Connick and Connie Liu from Sustainable Conservation and to Paula Trigueros and Marcia Brockbank from the San Francisco Estuary Project for their assistance and overall management of the project. Finally, we wish to acknowledge the helpful assistance provided by the reviewers of our draft work plan (Professor Thomas A. Cahill, University of California, Davis; Dr. Betty Pun, Atmospheric and Environmental Research, Inc.; Arne Anderson, Tribo-Diagnostics) and final report (Prof. Cahill; Dr. Pun; Dr. Moran; Glenis C. Lough, University of Wisconsin-Madison; Michael A. Robert, University of California, Davis; Kirsten Sinclair Rosselot, P.E., Process Profiles, Inc.).

Funding for this project has been provided in part through an Agreement with the State Water Resources Control Board (SWRCB) pursuant to the Costa-Machado Water Act of 2000 (Proposition 13) and any amendments thereto for the implementation of California's Nonpoint Source Pollution Control Program. The contents of this document do not necessarily reflect the views and policies of the SWRCB, nor does mention of trade names or commercial products constitute endorsement or recommendation for use.

1. EXECUTIVE SUMMARY

Characterization of airborne brake pad wear debris (BPWD) is one element of the Brake Pad Partnership's (BPP's) investigation of the environmental fate and transport of copper from automobile friction materials. The objective of the environmental transport and fate modeling is to predict how copper released from brake pads travels through the environment and its potential effect on the short-term and long-term concentrations of copper in the San Francisco Bay.

The primary objective of this task was to characterize airborne vehicle BPWD to provide input data needed to run an air deposition model. The air deposition model will calculate the transport of airborne BPWD generated from a representative brake pad formulation from the point of its origin to the points where the debris falls onto the watershed. Data input requirements for the air deposition model include average aerodynamic diameter, particle size distribution (PSD), and copper and iron contents for the representative airborne BPWD particles.

This Report describes the set of tasks completed and the resulting characterization of airborne BPWD from representative samples of three different brake pad materials. Samples of airborne BPWD were collected with a micro-orifice uniform deposition impactor (MOUDI) during generation of representative samples of BPWD on a brake dynamometer at Link Testing Laboratories in Detroit, using a standard BPWD generation protocol developed by the BPP. Advanced preparation for the sampling effort and post-sampling analyses were conducted at Clemson University.

Key findings from this study include:

- The generation of airborne BPWD was very different for the three different materials tested. In a typical 2.5 hour test cycle, the total net (i.e., background subtracted) average masses collected by the MOUDI were approximately 558, 955, and 76 µg for Materials A, B, and C, respectively.
- Background levels of airborne particulate matter in the testing facility proved to be much higher than anticipated, with an average total mass collected by the MOUDI approaching 101 µg for a typical 2.5 hour test cycle. These high background levels of airborne particulate matter appeared to be variable on a day-to-day basis, and may have been variable over even a much shorter time period. Presumably, the various tests being conducted on surrounding dynamometers in the facility led to these high measured background concentrations.
- The total net average copper (Cu) masses collected by the MOUDI were approximately 39, 45, and 4 µg for Materials A, B, and C, respectively, for the typical 2.5 hour test cycle. Therefore, this corresponds to average net Cu contents of approximately 7.0, 4.7, and 5.3% in the total airborne BPWD for Materials A, B, and C, respectively.
- The total net average iron (Fe) masses collected by the MOUDI were approximately 42 and 252 µg for Materials A and B, respectively, for the typical 2.5 hour test cycle. For Material C, the net average Fe mass was below detection. This corresponds to average net Fe contents of approximately 7.5 and 26.4 % in the total airborne BPWD for Materials A and B, respectively, and below detection for Material C.
- Based on a composition of 26.4% Material A, 14.1% Material B, and 59.5% Material C, the total net average mass that would have been collected by the MOUDI in a typical 2.5

hour test cycle for the hypothetical representative brake pad material was calculated to be approximately 328 µg. The total mass mean aerodynamic diameter of the airborne fraction of the hypothetical representative BPWD was calculated to be 5.3 ± 0.2 µm.

- For the same composition above, the corresponding mass mean aerodynamic diameters based on Cu and Fe contents were calculated to be 4.8 ± 0.4 µm and 4.8 ± 1.0 µm, respectively.
- The total net average Cu and Fe contents for the airborne fraction of the hypothetical representative BPWD were determined to be 5.8 ± 0.4 % and 14.8 ± 2.0 %, respectively.
- Characteristic values of the Cu-based aerodynamic particle size distribution for use with the fine grid air deposition model are: d_{50} = 3.5 µm, d_{25} = 1.5 µm, d_{75} = 5.6 µm.
- Characteristic values of the Cu-based aerodynamic particle size distribution for use with the coarse grid air deposition model are: d_{50} = 3.5 µm, with the lower and upper limits on d_{50} being 3.1 and 4.0 µm, respectively.

2. BACKGROUND

In a recent article, Sanders et al. (2003)[1] reported on work characterizing the size distribution of airborne brake wear debris. They found that the mass mean diameter of the brake wear debris they tested was 6 µm, while essentially all the mass of brake wear debris was contained within the range of 1 to 30 µm. Iron (Fe), copper (Cu), and barium (Ba) were the three predominant elements identified in the brake wear debris, regardless of the material used in the brake lining. The size distributions obtained in the Sanders study, however, may have been influenced by the testing protocol used, such that there may well be a significant amount of material with a size of less than 1 µm. For example, in an earlier study by Garg et al. (2000)[2], the mass median diameter of brake wear debris was found to be smaller than that measured by Sanders et al. (2003), and ranged from 0.5 to 2.5 µm.

After discussion with the BPP Steering Committee and air deposition modelers, it was determined that the best approach would be to use a micro-orifice uniform deposition impactor (MOUDI) to determine the aerodynamic diameters and particle size distributions of the airborne brake wear debris particles. These impactors operate at an airflow rate of 30 liters per minute (lpm) and typically have eleven stages, with aerodynamic diameter cutoffs ranging from 0.056 to 18 µm. A downstream filter collects particles that escape the MOUDI (i.e., particles smaller than 0.056 µm in diameter).

MOUDI analyzers were first described by Marple et al. (1991)[3], and are very well-characterized instruments. They have been successfully used in many projects since becoming commercially available.

---

[1] P.G. Sanders, N. Xu, T.M. Dalka, and M. Maricq (2003) "Airborne Brake Wear Debris: Size Distributions, Composition, and a Comparison of Dynamometer and Vehicle Tests," *Environ. Sci. Technol.,* **37**, 4060-4069.

[2] B.D. Garg, S.H. Cadle, P.A. Mulawa, P.J. Groblicki, C. Laroo, and G.A. Parr (2000) "Brake wear particulate matter emissions," *Environ. Sci. Technol.,* **34**, 4463-4469.

[3] V.A. Marple, K.L. Rubow, and S.M. Behm, (1991) "A Microorifice Uniform Deposit Impactor (MOUDI) - Description, Calibration, And Use," *Aerosol Sci. Technol.,* **14 (4),** 434-446.

3. AIRBORNE BRAKE WEAR DEBRIS SAMPLING

3a. Achieving Isokinetic Sampling Conditions

Sampling instruments require isokinetic sampling conditions—i.e., it is necessary that the velocities of the air flow in the dynamometer ductwork and in the probe (the inlet to the MOUDI) be close to one another, usually within 10%. The reason for this is to ensure that the sample is fully representative of the particles suspended in air. Particles, because of their inertia, do not necessarily follow bending air streamlines. If the velocity of the duct air is significantly higher than the air velocity in the probe, the streamlines must diverge around the probe. Larger particles, because of their inertia, will tend to go straight, and therefore additional particles will enter the sampling probe, introducing a bias in the measurement. In this case, the measurement will show a higher mass concentration than actual. If the velocity of the duct air is less than the air velocity in the probe, the streamlines must converge into the probe. Particles, because of their inertia, will tend to go straight and therefore miss the sampling probe, again introducing a bias in the measurement. In this case, the measurement will show a lower than actual mass concentration. Perhaps even more importantly for the current project, the measured particle size distributions would not have been accurate because larger particles are more likely than smaller particles to cross streamlines when isokinetic sampling conditions are not maintained.

Measurements and information available from a previous test using the same dynamometer protocol[4] indicated that the speed of the air inside the dynamometer duct at the location of the inlet probe was about 5 miles per hour (low of 3 mph and high of 8 mph), or approximately 134.4 m/min. Since the inlet to the MOUDI requires an air flow close to 30 lpm, to achieve velocities comparative to 134.4 m/min a sample probe area equal to

$$Area = \frac{flow}{velocity} = \frac{30 \times 10^{-3} m^3 / \min}{134.4 \ m / \min} = 2.23 \times 10^{-4} m^2$$

was needed. This meant that the inlet pipe to the MOUDI required an inner diameter (ID) of approximately 0.017 m (17 mm).

3b. Sampling Equipment Setup

A Schedule 40 nominal 2-inch PVC pipe, which served as the inlet to the high volume sample filter used in tests conducted by the LINK engineers, was installed in the dynamometer ductwork (Figure 1 and Appendix A). This location was selected as the most convenient inlet for placing any particulate sampling equipment. A stainless steel tube with an approximately 17 mm inside diameter was inserted through the PVC pipe that served as the inlet to (i.e., sampling probe for) the MOUDI. This tube was held in place at both ends of the existing PVC pipe with plexiglass collars. In addition to holding the inner tube in place, the collars served to seal the annulus region between the PVC pipe and inner tube. The leading edge of the stainless steel tube was

---

[4] Brake Manufacturers Council Product Environmental Committee, *Disc Brake Wear Debris Generation and Characterization: A Dynamometer Based Protocol for Generating and Collecting Vehicle Disc Brake Wear Debris,* prepared by James T. Trainor, May 15, 2001.

ground with a shallow conical bevel, such that it provided minimal disruption to the air flow. The rear end of the stainless steel tube was electrically grounded to the MOUDI frame to dissipate any electrostatic charge. With this sampling scheme, changeovers between the MOUDI device and the normal high volume filter were accomplished rapidly, thereby requiring only a minimum amount of downtime during any one brake wear debris sampling run. This sampling scheme maintained isokinetic sampling for the MOUDI device and minimized the degree to which the dynamometer was modified from its originally designed specifications.

Before leaving Clemson, a 90 degree bend was made in the sampling probe to connect the horizontal sampling inlet to the vertical MOUDI inlet based on pictures available from Trainor's report[4] (see Appendix A). Upon arrival at Link, however, it was found that the dynamometer was different from the one used previously, and the dynamometer ductwork in the test setup was lower to the ground than originally anticipated. It was not possible to connect the MOUDI at this level due to its height, so additional bends in the sampling tube were made to accommodate the height difference. This setup was selected after careful consideration of several options, including the use of a flexible teflon or stainless steel hose. However, the use of either hose setup would have required additional connections between the hose and pipe fittings on the MOUDI as well as the sampling probe. In addition, it also would have required a support system to maintain the shape of the tubing and ensure consistent sampling conditions from run to run. The bent tube connection was selected for its simplicity, ease of handling, and minimal effect on the sampled flow. The final MOUDI connection is shown in Figure 1.

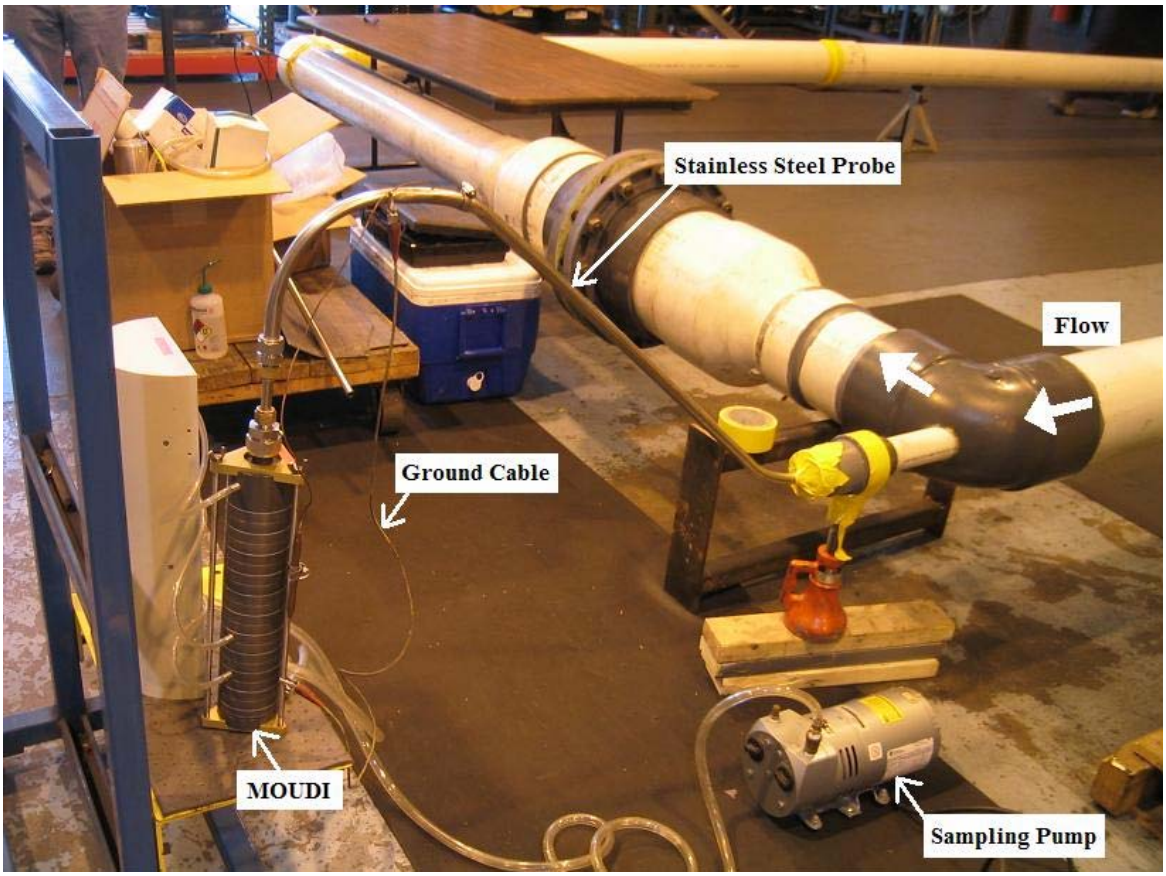

Figure 1: Brake Pad Material Sampling Equipment Setup

3c. Coordinating with the Effort to Generate the Representative Sample of Wear Debris

The airborne wear debris sampling was performed in conjunction with the effort to generate a representative sample of non-airborne brake wear debris, which required close coordination with Link Testing Laboratory and the industry members of the BPP Steering Committee who led the representative sample generation effort. The steps below outline how the airborne wear debris sampling was conducted in conjunction with the effort to generate a representative sample of non-airborne wear debris. This plan was selected based on the industry members' workplan to generate the brake wear debris and discussion of such workplan by the BPP Steering Committee members.

Link engineers were able to generate enough non-airborne brake wear debris for each brake pad material to meet the needs of the industry members' planned solubility and leaching studies by running the dynamometer test approximately 22 hours (8 or more dynamometer cycles of 298 stops each) following the established protocol.[4] The testing of all three brake pad formulations was completed in approximately four days (June 28 – July 2, 2004), and the Clemson team completed all of their MOUDI measurements in this same time period.

3d. Collecting Replicate Samples and Blanks

Prior to the arrival of the Clemson team, Link engineers burnished each brake pad material following the protocol's standard burnishing procedure. Then, a blank MOUDI run was conducted to determine the background particle concentration of the air being pulled through the experimental setup. Upon completion of the blank run the MOUDI sampler was replaced with a second MOUDI preloaded with filters, and Link engineers commenced generating brake wear debris following the established protocol.[4] This protocol consists of a 298 brake application cycle that was repeated eight or more times. At an appropriate time within the protocol run (e.g., completion of a full cycle), the Link engineers stopped the run so that the Clemson team could change out the MOUDI sampler as described above. The engineers then restarted the run for another full cycle, at which point they again stopped the run so that the Clemson team could change out the MOUDI sampler. At the end of three consecutive cycles, the MOUDI sample probe was completely removed from the PVC pipe and the high volume sampler was connected to finish out the remaining approximately 5 cycles of the entire dynamometer run.

In a previous test using the same dynamometer protocol,[4] 2.38 grams of airborne BPWD were generated over the course of 8.5 dynamometer cycles, which took approximately 18 total hours of dynamometer run time. Based on this information, the Clemson team estimated that one full dynamometer cycle would be sufficient to generate enough material to determine the physicochemical characteristics of the airborne BPWD. However, this calculation was based on two important assumptions: (1) that the airborne BPWD generation rates for the three materials to be tested would be roughly equivalent to the one previous material tested, and (2) that the background particle concentrations in the test facility would be negligible. As will be shown later, these two assumptions were not necessarily observed. Three replicate samples for each brake pad material were collected, and each MOUDI replicate measurement was conducted on one full dynamometer cycle.

As noted above, prior to the generation test for each brake pad material, the MOUDI sampler was installed and an ~2 hour blank sample was collected to determine whether the HEPA filter installed on the dynamometer's airflow system was allowing an appreciable mass of background particles to pass the filter. Based on the filter's design performance of 99.7% capture efficiency for > 0.3 micron sized particles, this was not expected. However, if the background particle concentrations were appreciable, then the blank sample particle masses associated with each MOUDI size cut would have to be subtracted from the actual samples.

Upon completion of a particular MOUDI sample/blank run, the impactor was disassembled and the filters removed and placed into premarked containers for mass determinations back at Clemson University as described below. New preweighed filters were then removed from their marked containers and loaded in the MOUDI sampler, which was reassembled in preparation for its next sample measurement.

4. GRAVIMETRIC ANALYSIS

Gravimetric analysis was used to determine the total mass of brake wear debris collected on the Teflon filters of the MOUDI analyzer. Each filter was weighed before and after sampling, and the total mass collected on the filter was determined by the difference. The mass of brake wear debris collected on each stage/filter was then used to determine the particle concentration in the air by dividing the mass collected by the total volume of sampled air. This approach is a convenient means to normalize the data for all runs which had slightly different run times, as well as to subtract the blank/background particle concentrations.

Teflon filters were weighed on a Mettler-Toledo UMT-2 microbalance, which has a maximum capacity of 2.1 mg and a display precision of 0.1 μg. Gravimetric analysis of samples as small as those which were collected is subject to a number of obstacles, such as mechanical vibrations, air currents, static charge on the filters, and temperature and relative humidity variations. One in every five filters was re-weighed to ensure that varying weighing conditions did not affect the measurements. The weighing chamber of the UMT-2 microbalance is enclosed to avoid the effects of air currents, and the balance is designed to dampen mechanical vibrations. Throughout the gravimetric analysis procedure, the room was maintained at 75 ± 5 °F and 45 ± 5% relative humidity.

5. POST-SAMPLING ANALYSIS

As described above, the exposed filters were weighed to determine the concentration size distribution. Additional analysis of the airborne brake wear debris samples included determination of element/metals content of the material captured on the filters.

The copper and iron contents of the collected airborne brake wear debris were analyzed after microwave-assisted acid digestion by inductively coupled plasma-atomic emission spectroscopy (ICP/AES), following the procedures previously developed for non-airborne BPWD.[5]

[5] J. Hur, S. Yim, and M. Schlautman (2003) “Copper leaching from brake wear debris in standard extraction solutions," *J. Env. Monit.*, **5**, 837-843.

Finally, based on percentage values provided by the industry members of the BPP for the three different brake pad materials tested, the physiochemical characteristics for the hypothetical airborne fraction of the representative BPWD sample was calculated. This final result provided the airborne characteristics for the BPWD to complement the non-airborne BPWD representative sample that is being generated for the overall project.

6. RESULTS OF GRAVIMETRIC ANALYSIS

6a. Aerodynamic Particle Size Distributions and Data Evaluation Processes

To account for differences in sampling time for each run, the aerodynamic particle size distribution data were expressed on a concentration basis. Total flow through the MOUDI for each sampling run was determined by multiplying the volumetric flow (30 liters per minute, lpm) by the specific sampling time for each run. The concentration of particles from each size bin was then determined by dividing the mass accumulated on an individual filter by the total flow through the MOUDI for the corresponding run. Concentrations were calculated as

$$Concentration = \frac{(final\ \ filter\ \ weight - initial\ \ filter\ \ weight)}{(30\ \ lpm)\ \times\ (sampling\ \ time\ \ in\ \ minutes)}$$

The aerodynamic particle size distribution data were also expressed as a mass accumulation over a constant fixed time period of 2.5 hours. These normalized masses were calculated as

$$Mass\ \ per\ \ 2.5\ \ hours = Concentration\ \times\ (30\ \ lpm)\ \times\ (150\ \ minutes)$$

Concentration and normalized mass were plotted against geometric mean particle diameter for each size bin. The geometric mean particle diameter was calculated from the upper and lower cutoff values as

$$Geometric\ \ Mean\ \ Diameter = \sqrt{(Upper\ \ Cutoff\ \ \ Diameter)\ \ \times\ \ (Lower\ \ Cutoff\ \ \ Diameter)}$$

The aerodynamic particle size distribution data for all MOUDI runs (i.e., triplicate measurements for blank samples and brake pad Materials A, B, and C) are plotted in Figure 2. Data points which were calculated as negative mass accumulations from the gravimetric measurement analysis are shown here as zeros because of the physical impossibility of negative mass accumulation. Instead, such results likely reflect low mass accumulations that were less than the uncertainty associated with the filter weighing process itself. These individual data points were excluded from all subsequent analyses and calculations. All raw data used to generate Figure 2 are given in Appendix C.

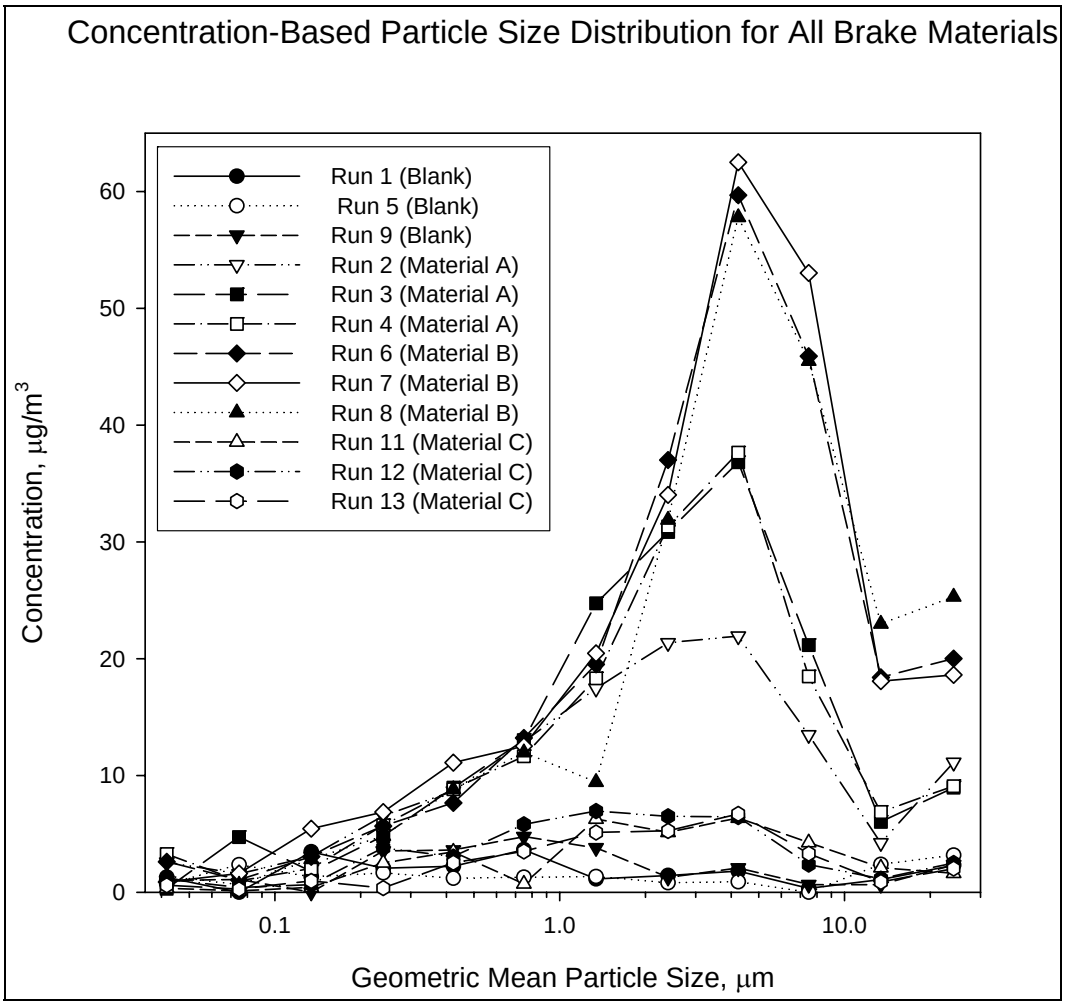

Figure 2: Particle Size Distributions for Materials A, B, and C and Blank Runs

Discrete and cumulative aerodynamic particle size distributions for the blank/background runs are shown in Figures 3 and 4, respectively. The background particle concentrations were appreciable and appeared to vary from day to day, presumably due to the surrounding activities occurring in the Link testing facilities or debris that had remained inside the ductwork from previous runs. In addition, it is difficult to ascertain whether the variability in background particle concentrations was occurring on a more frequent time frame (e.g., during a particular MOUDI run).

The surrounding environment at Link's testing facilities consisted of several dynamometers operating independently of our tests, so improper sealing of the dynamometer may have allowed some air to enter the chamber directly rather than forcing it to pass though the HEPA filter. The background sampling conditions may have been variable not only from day to day but also from hour to hour. Therefore, the particle size distributions for Materials A, B, and C were compared to an averaged background level while recognizing that the actual background levels during any particular run may have varied slightly from this average.

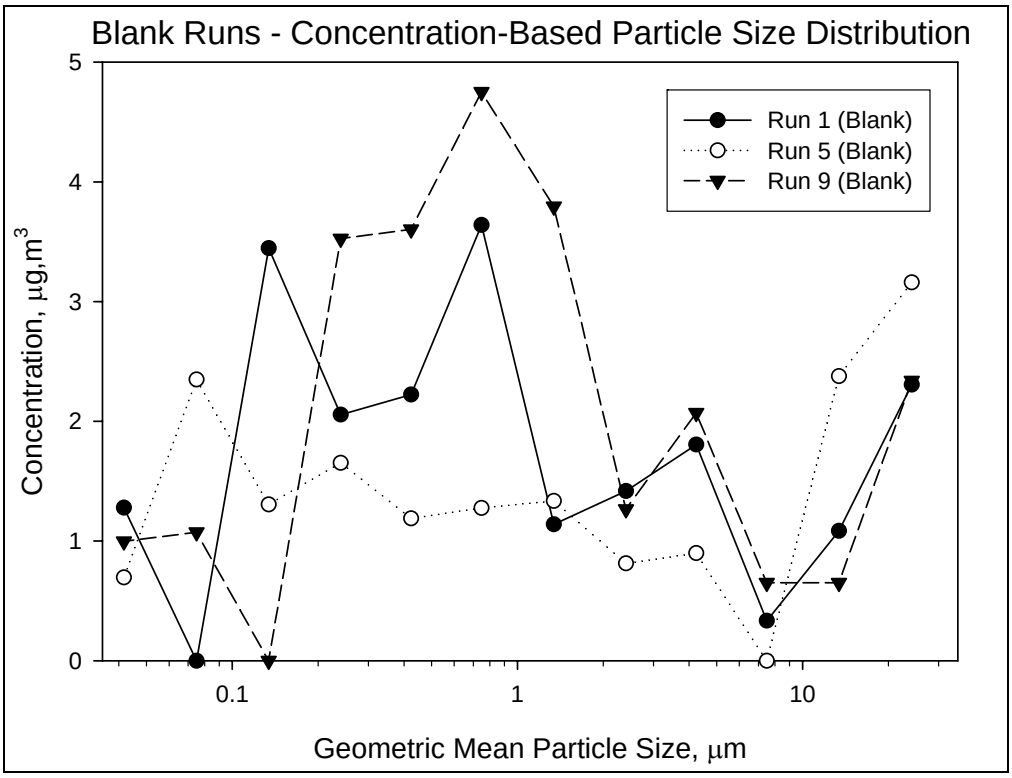

Figure 3: Particle Size Distribution for the Blank Runs

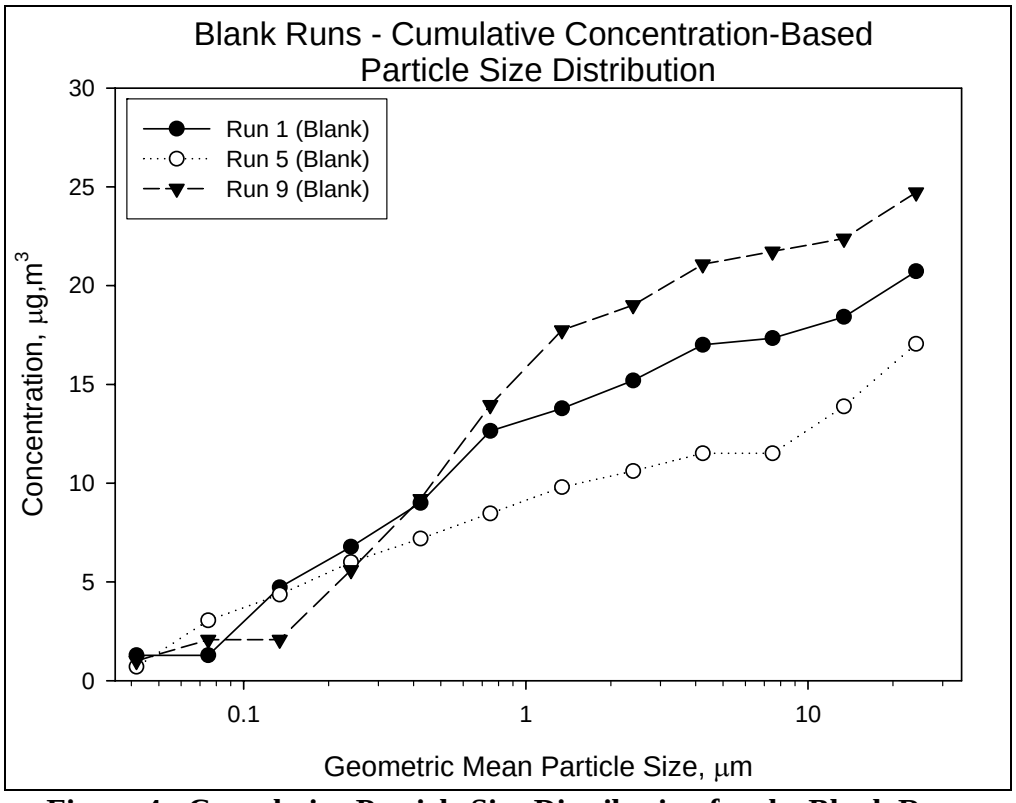

Figure 4: Cumulative Particle Size Distribution for the Blank Runs

The discrete and cumulative aerodynamic particle size distributions for Material A relative to the average background are shown in Figures 5 and 6, respectively. Analogous distributions for Materials B and C are presented in Figures 7 and 8 and in Figures 9 and 10, respectively.

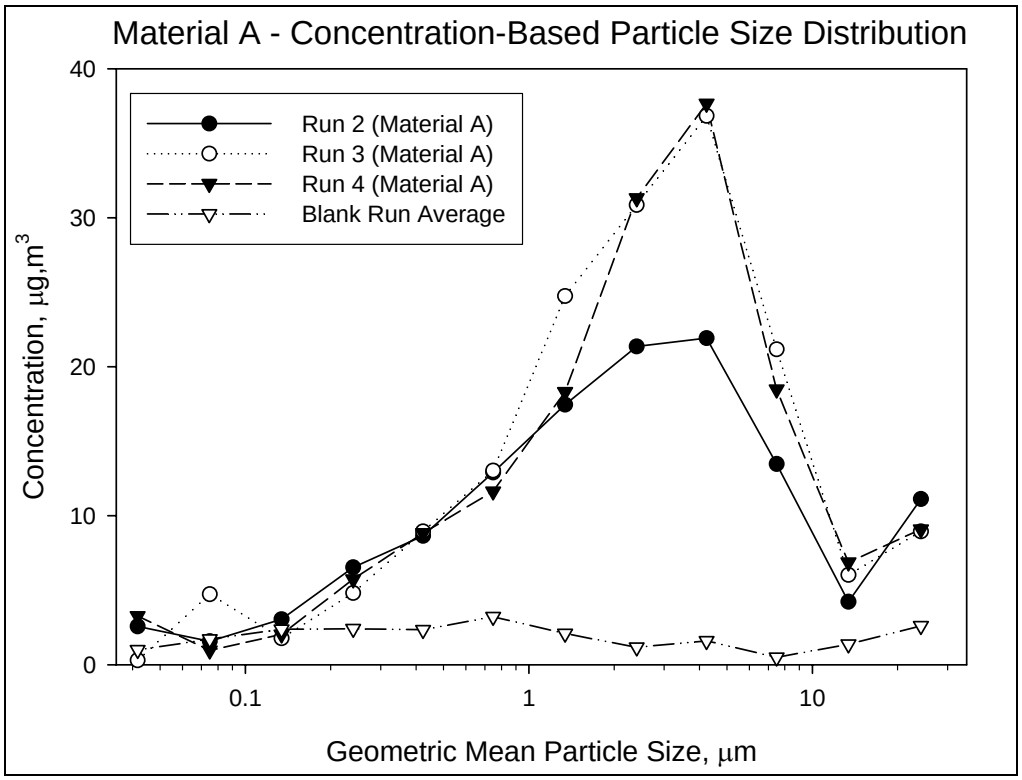

Figure 5: Particle Size Distribution for Material A

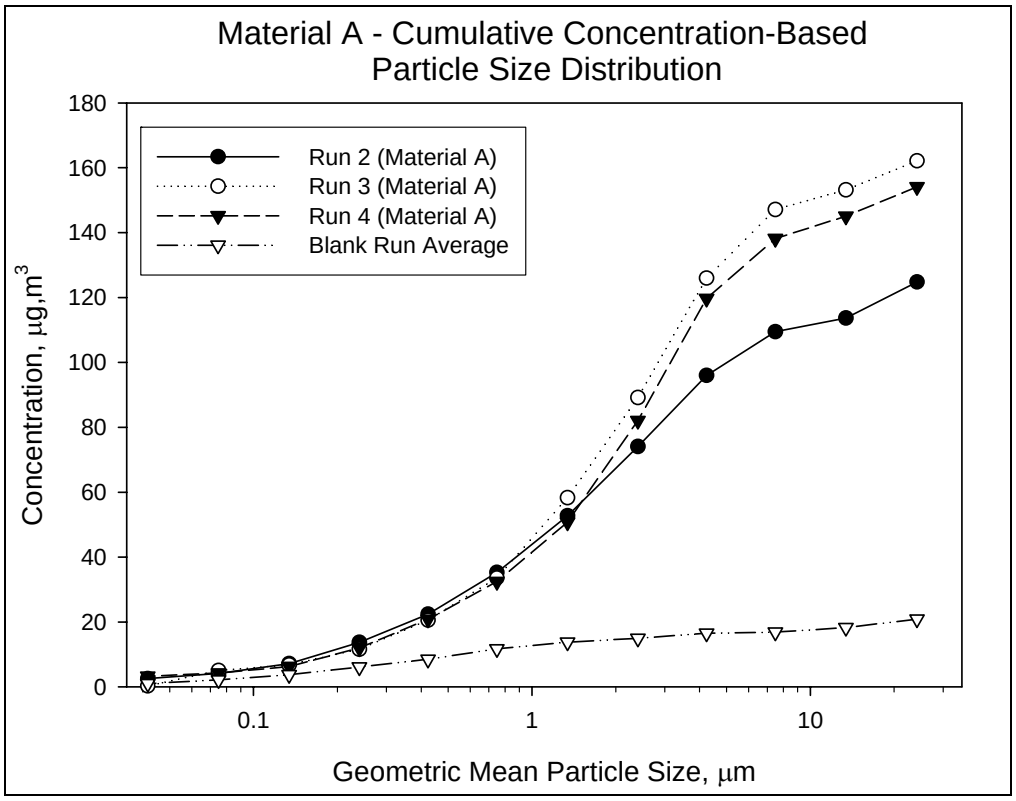

Figure 6: Cumulative Particle Size Distribution for Material A

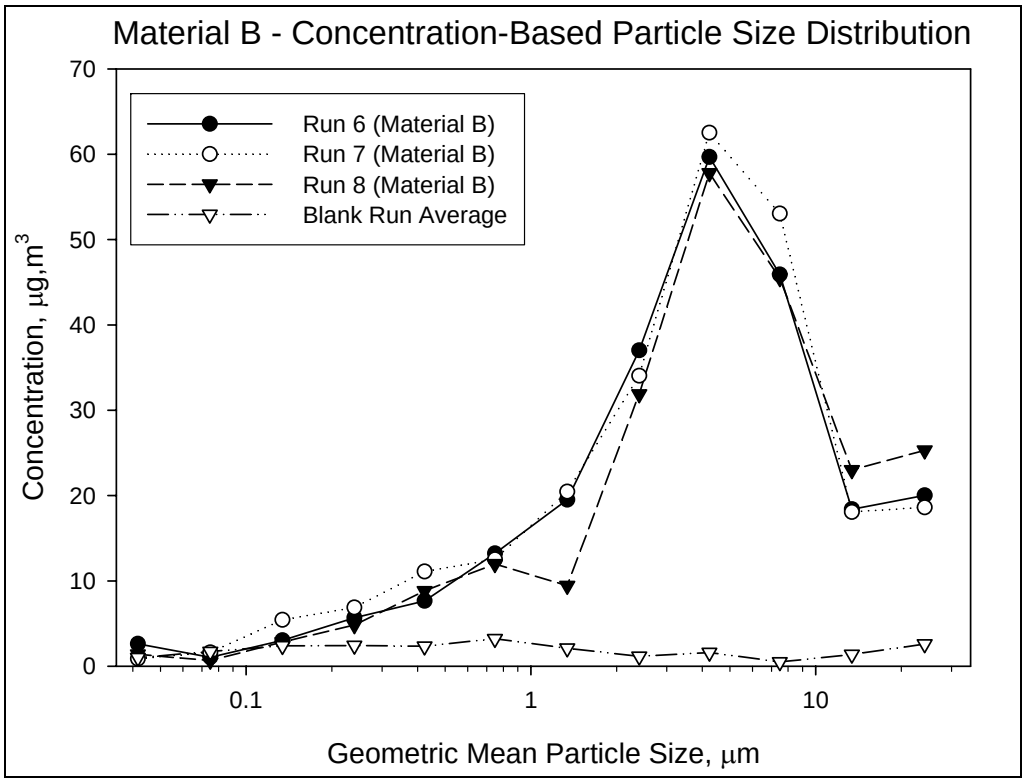

Figure 7: Particle Size Distribution for Material B

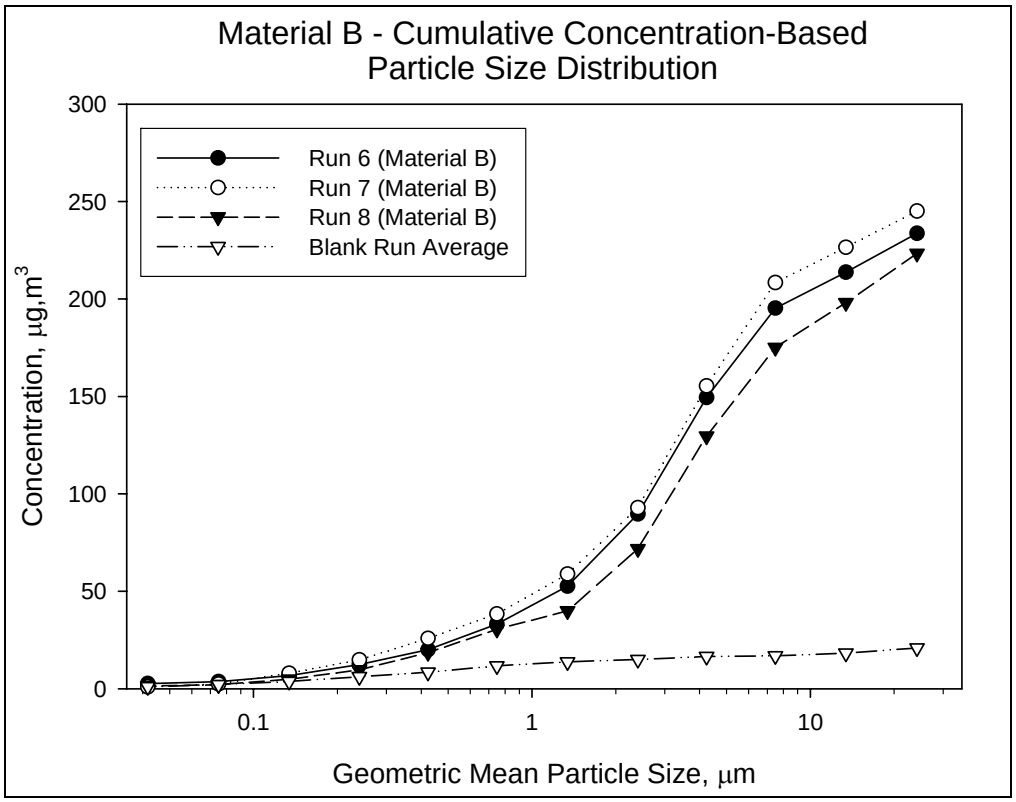

Figure 8: Cumulative Particle Size Distribution for Material B

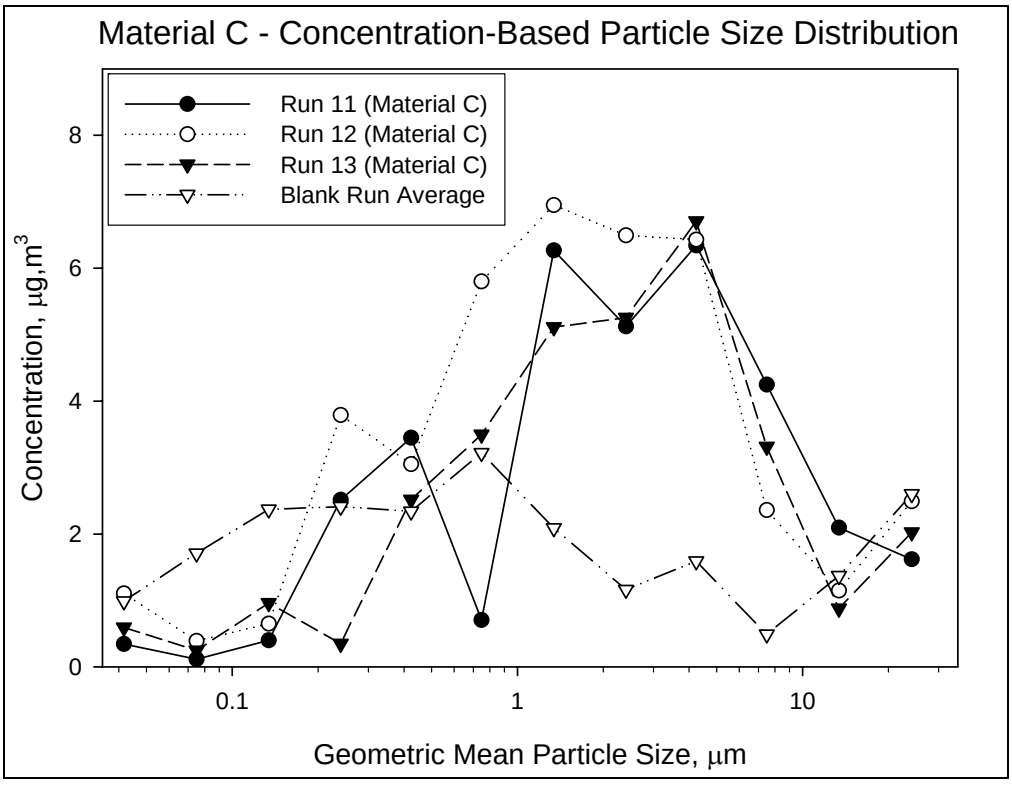

Figure 9: Particle Size Distribution for Material C

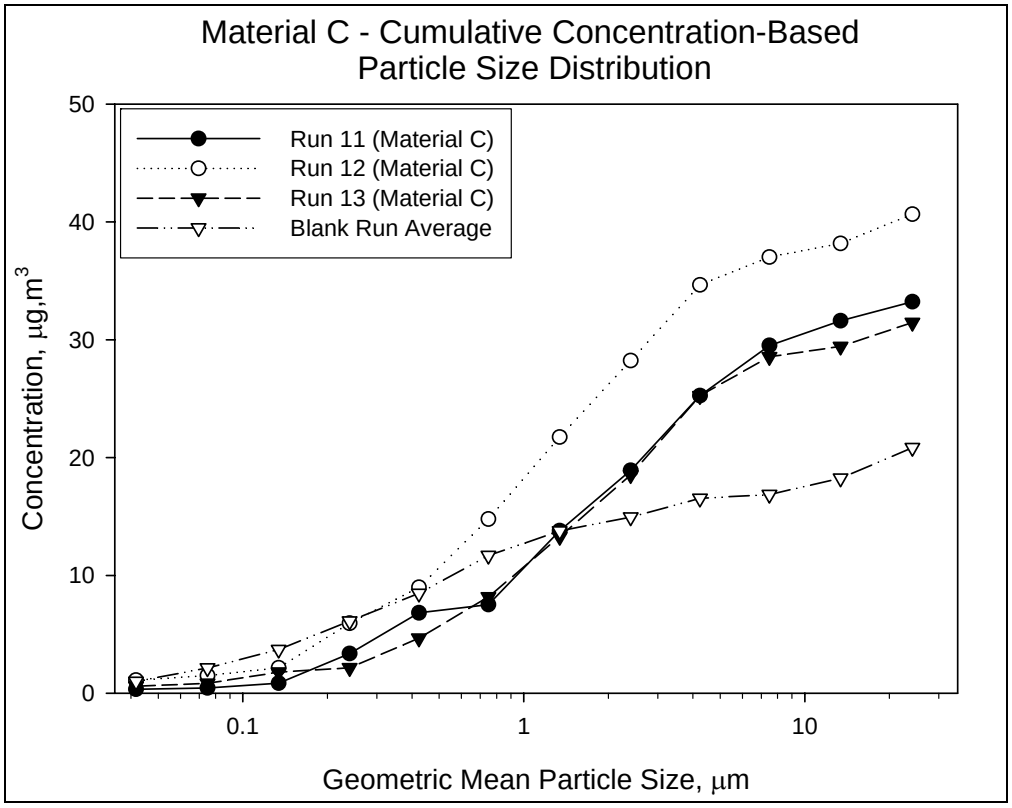

Figure 10: Cumulative Particle Size Distribution for Material C

6b. Calculation of Aerodynamic Particle Size Distributions for the Composite Sample

For each brake pad material, the net average concentration within each MOUDI size bin was determined, and the standard errors associated with these calculations were evaluated. Instrument uncertainties are not known and therefore are not included in these calculations. However, these uncertainties are expected to be well below the variability between consecutive runs of a material. The net average concentrations were calculated as:

$$Net\ \ Average\ \ Concentration =$$
$$(Average\ \ Concentration\ \ for\ \ a\ \ Material)\ -\ (Average\ \ Blank\ \ Concentration)$$

Negative values for net average concentration were taken as zero because these values were impossible and likely the result of high and/or variable background interferences.

The standard error associated with the net average concentration of a material was calculated by error propagation using the Root Sum Square method, and the standard errors associated with the average concentration for a material and the average blank concentration were calculated as:

$$SE_{(Average\ \ Concentration)} = (Standard\ \ Deviation) \div \sqrt{(Number\ of\ \ Runs)}$$

$$SE_{(Net\ \ Average\ \ Concentration)} = \sqrt{SE^2_{(Average\ \ Concentration\ \ for\ \ a\ \ Material)} + SE^2_{(Average\ \ Blank\ \ Concentration)}}$$

These data for net average concentrations then were used to calculate discrete and cumulative particle size distributions for the hypothetical composite airborne sample by the prescribed rubric:

$$Net\ \ Composite\ \ Average =$$
$$(0.264) \times (Net\ \ Average\ \ A) + (0.141) \times (Net\ \ Average\ \ B) + (0.595) \times (Net\ \ Average\ \ C)$$

where 0.264, 0.141, and 0.595 correspond to the composition values provided by the industry members for the relative fractions corresponding to Materials A, B, and C, respectively. The standard error associated with the net composite average was calculated as:

$$SE_{(Net\ \ Composite\ \ Average)} =$$
$$\sqrt{[(0.264) \times SE_{(Net\ \ Average\ \ A)}]^2 + [(0.141) \times SE_{(Net\ \ Average\ \ B)}]^2 + [(0.595) \times SE_{(Net\ \ Average\ \ C)}]^2}$$

The discrete and cumulative net average aerodynamic particle size distributions and associated uncertainties are shown in Figures 11 and 12, respectively, for Materials A, B, and C. The discrete and cumulative net average aerodynamic particle size distributions and associated uncertainties are shown in Figures 13 and 14, respectively, for the airborne fraction of the representative BPWD sample. Particle size distribution data for the composite sample are given in Table 1 in Appendix B. Characteristic values associated with this mass-based composite particle size distribution appropriate for modeling purposes are provided in Appendix E.

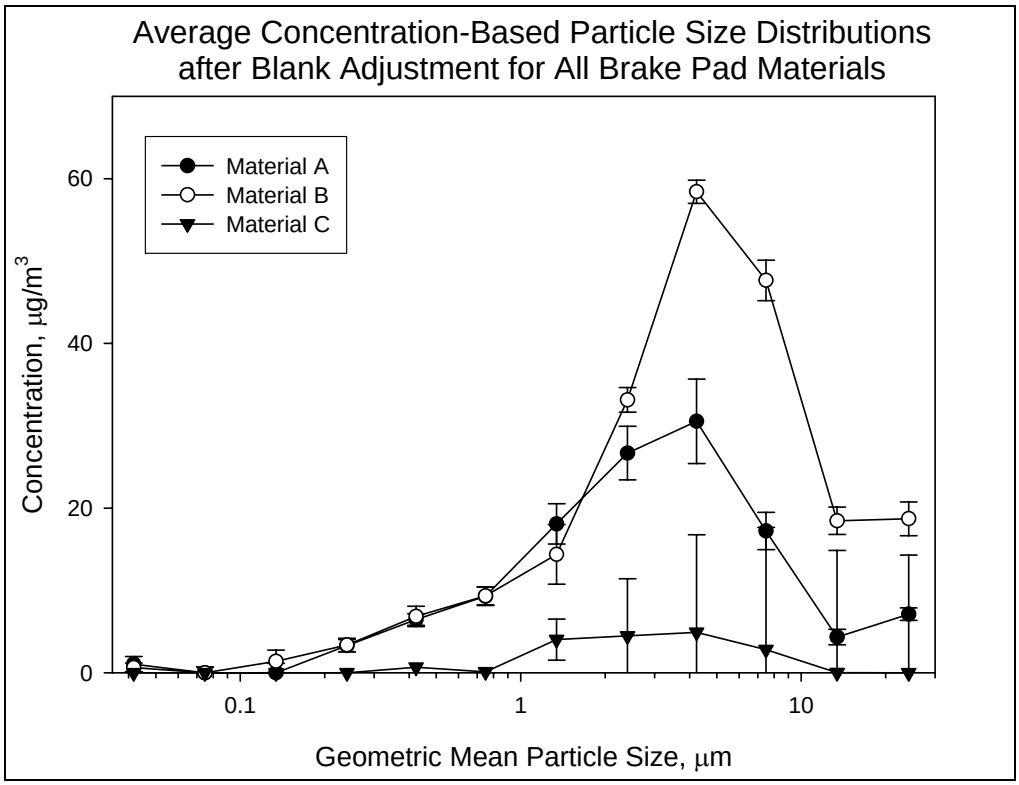

Figure 11: Net Average Particle Size Distributions for Materials A, B, and C

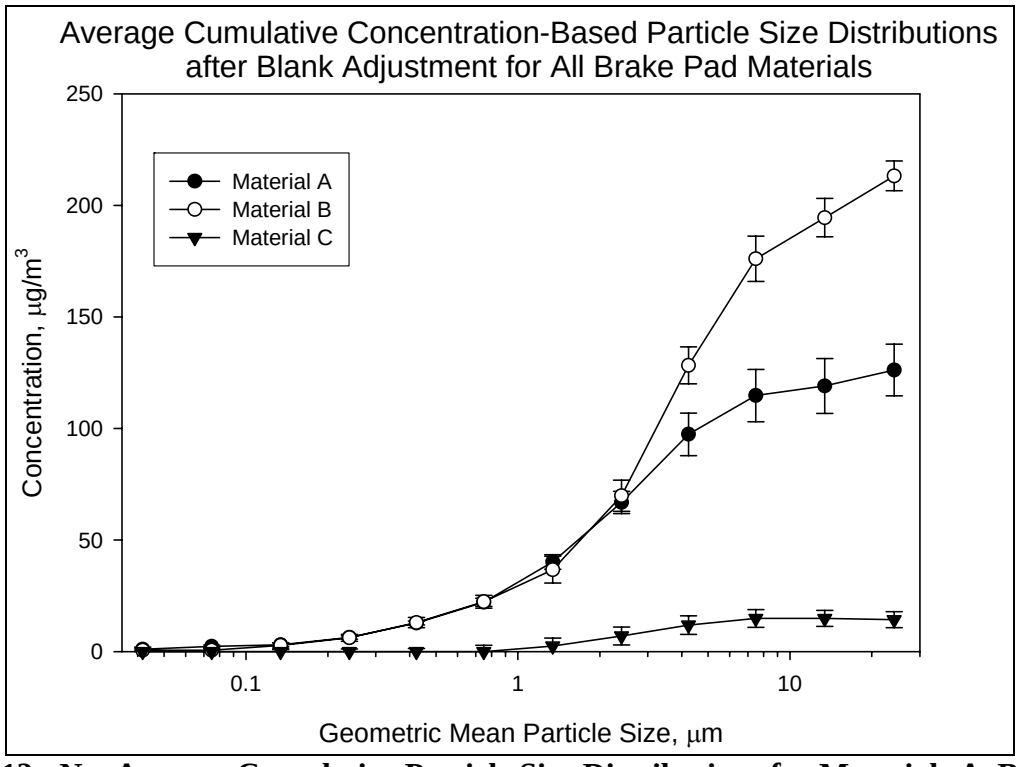

Figure 12: Net Average Cumulative Particle Size Distributions for Materials A, B, and C

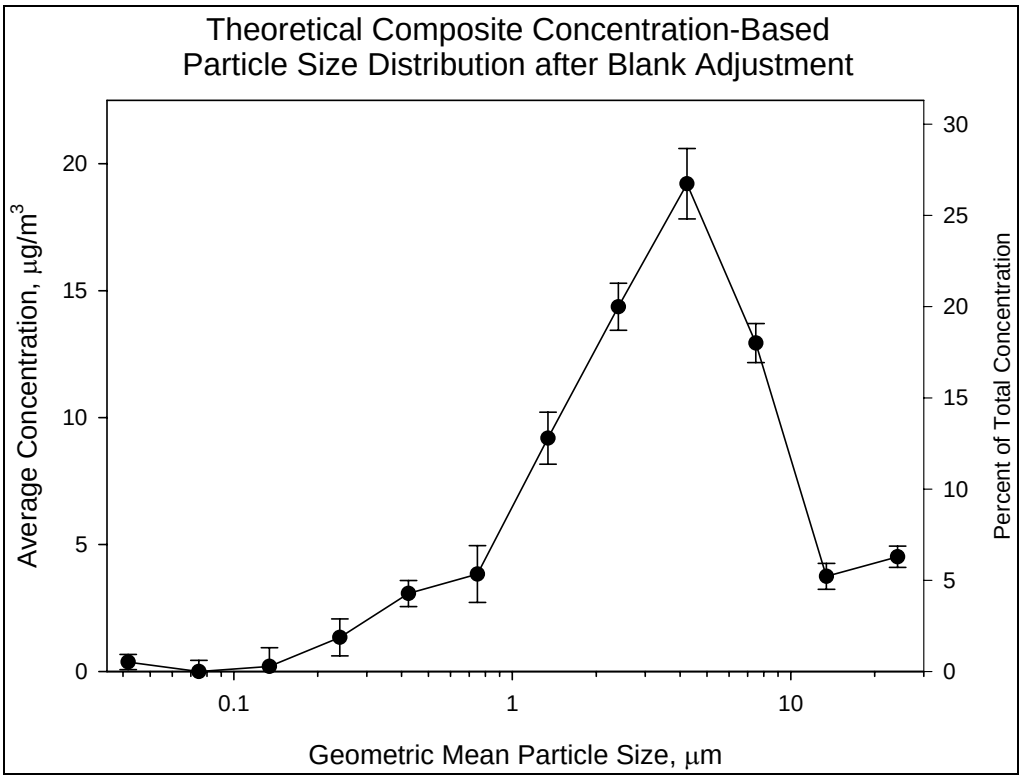

Figure 13: Particle Size Distribution for Hypothetical Composite Material

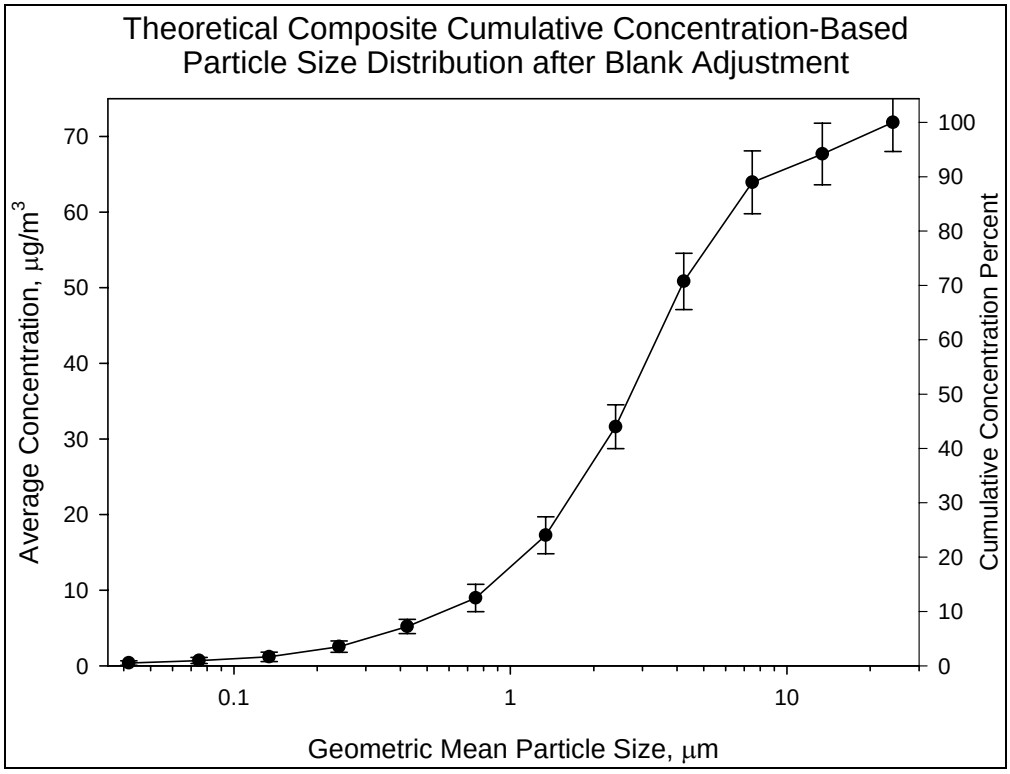

Figure 14: Cumulative Particle Size Distribution for Hypothetical Composite Material

6c. Calculation of the Aerodynamic Mass Mean Diameter for the Composite Sample

From the particle size distribution data, the mass mean diameter of the hypothetical composite sample was calculated along with its associated standard error via error propagation. Absolute uncertainties in the cutoff diameters associated with the MOUDI stages were not known and thus not included in the calculations. However, these uncertainties are expected to be well below the uncertainties resulting from the replicate gravimetric data.

The mass mean diameter was calculated as:

$$Mass\ \ Mean\ \ Diameter = \frac{\sum[(Net\ \ Accumulation\ \ per\ \ Size\ \ Bin)\times(Geometric\ \ Mean\ \ Diameter)]}{Total\ \ Net\ \ Accumulation}$$

The standard error associated with the mass mean diameter of the composite sample was calculated by error propagation by adding fractional uncertainties in quadrature and multiplying this overall fractional uncertainty by the mass mean diameter as:

$$SE(Mass\ \ Mean\ \ Diameter) = (Mass\ \ Mean\ \ Diameter)\times$$

$$\sqrt{\left(\frac{SE(\sum[(Net\ Accumulation\ per\ Size\ Bin)\times(Geometric\ Mean\ Diameter)])}{\sum[(Net\ \ Accumulation\ \ per\ \ Size\ \ Bin)\times(Geometric\ \ Mean\ \ Diameter)]}\right)^2 + \left(\frac{SE(Total\ \ Net\ \ Accumulation)}{Total\ \ Net\ \ Accumulation}\right)^2}$$

where the standard error associated with the sum of the product of the net accumulation per size bin and the geometric mean diameter of that size bin was calculated as:

$$SE(\sum[(Net\ \ Accumulation\ \ per\ \ Size\ \ Bin)\times(Geometric\ \ Mean\ \ Diameter)]) =$$

$$\sqrt{\sum\left[[(Net\ \ Accumulation\ \ per\ \ Size\ \ Bin)\times(Geometric\ \ Mean\ \ Diameter)]\times(Fractional\ \ Uncertainty)^2\right]^2}$$

where the fractional uncertainty associated with the net accumulation in each size bin was calculated as:

$$Fractional\ \ Uncertainty = \frac{SE(Net\ \ Accumulation\ \ per\ \ Size\ \ Bin)}{(Net\ \ Accumulation\ \ per\ \ Size\ \ Bin)}$$

and where the standard error associated with the total net accumulation was calculated as:

$$SE(\sum Net\ \ Accumulation) = \sqrt{\sum[SE(Net\ \ Accumulation\ \ per\ \ Size\ \ Bin)]^2}$$

Using the equations above and the data in Table 1 from Appendix B, the aerodynamic mass mean diameter for the theoretical composite sample was determined to be 5.3 ± 0.2 μm.

7. RESULTS OF POST-SAMPLING ANALYSIS

7a. Aerodynamic Particle Size Distributions Based on Copper Analysis

The distributions of Cu for all MOUDI runs are presented in Figure 15. All data used to generate Figure 15 are given in Table 4 of Appendix C. Discrete and cumulative Cu distributions for the blank/background MOUDI runs are shown in Figures 16 and 17, respectively. Consistent with the total mass-based particle size distribution data shown in Section 6a, variability was evident in the background Cu measurements. An average background Cu distribution was calculated from the three replicate background measurements, and an average Cu content of approximately 7.4% was calculated for the background particle concentrations. Discrete and cumulative Cu distributions for Material A relative to the average Cu background are shown in Figures 18 and 19, respectively. Analogous Cu distributions for Materials B and C are presented in Figures 20 and 21 and in Figures 22 and 23, respectively.

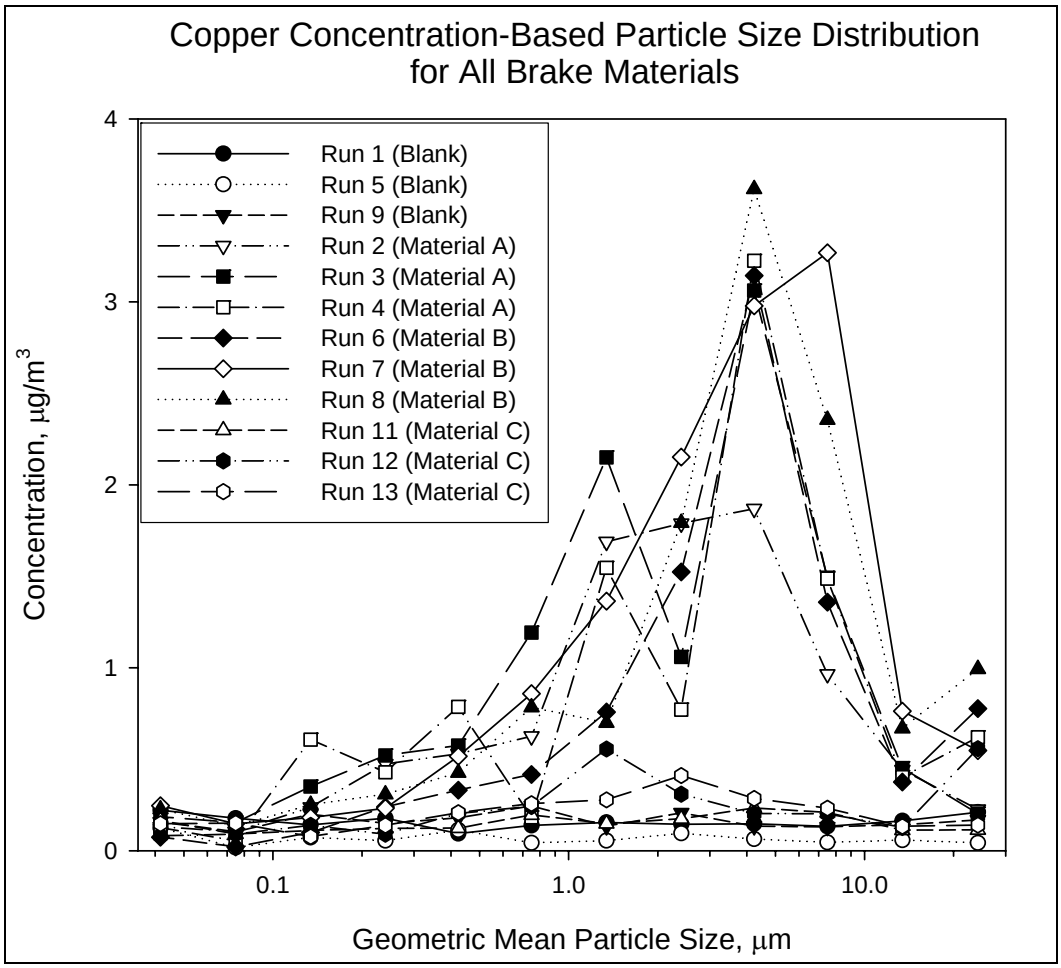

Figure 15: Copper Particle Size Distributions for Materials A, B, and C and Blank Runs

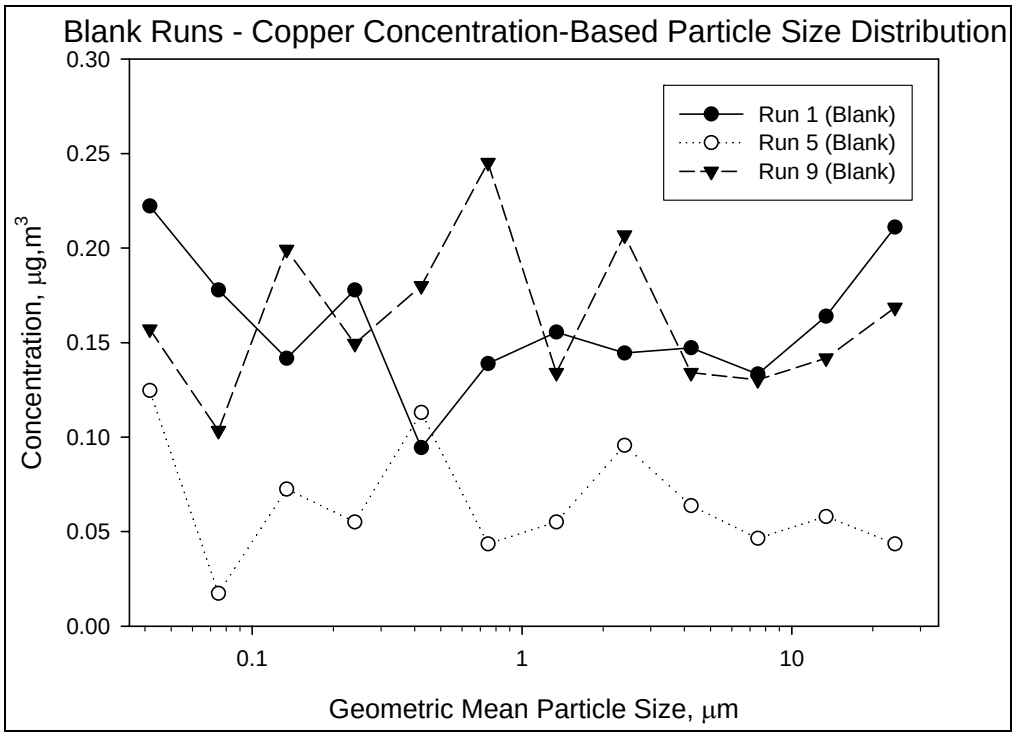

Figure 16: Copper Particle Size Distribution for the Blank Runs

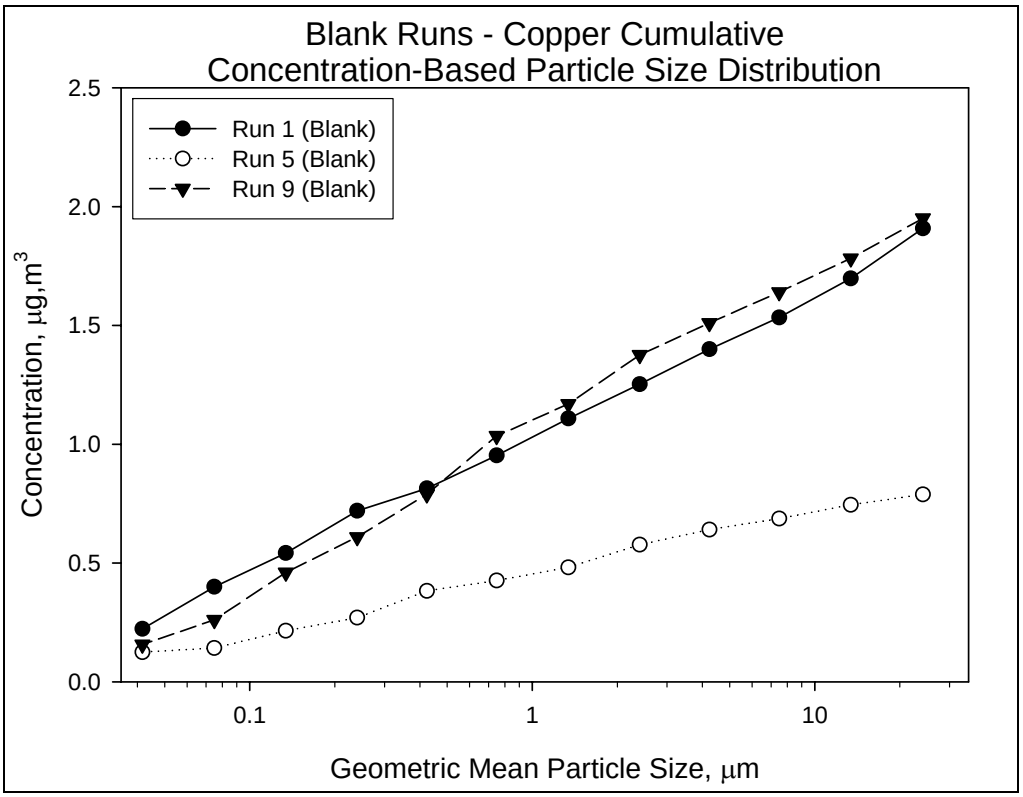

Figure 17: Cumulative Copper Particle Size Distribution for the Blank Runs

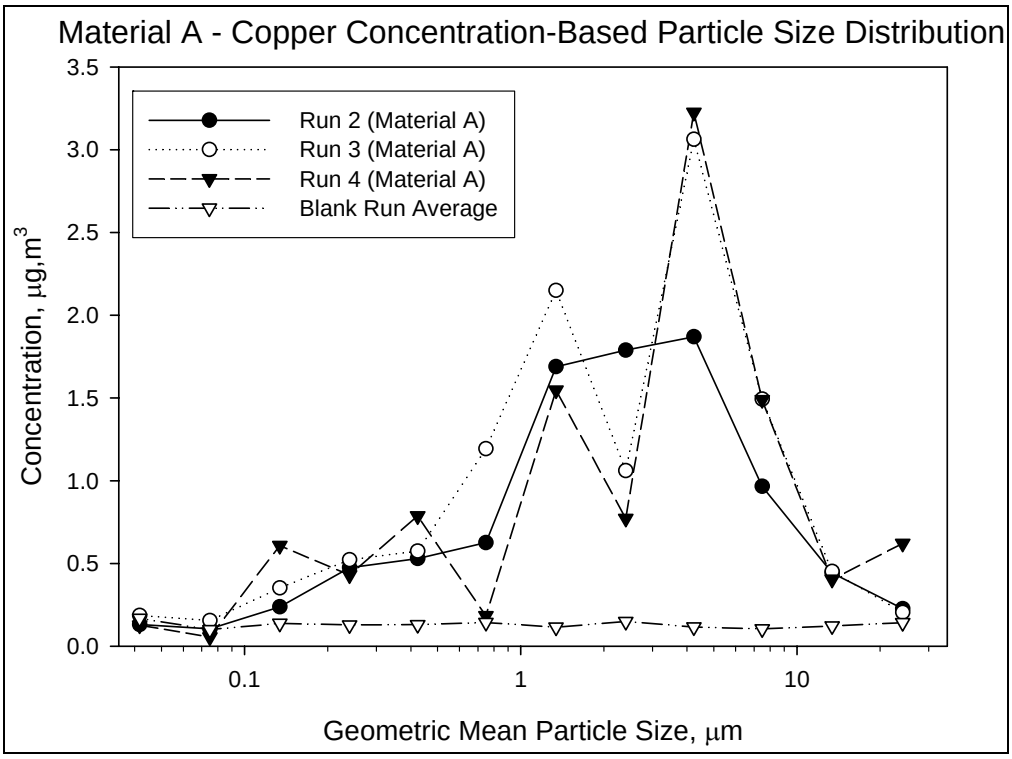

Figure 18: Copper Particle Size Distribution for Material A

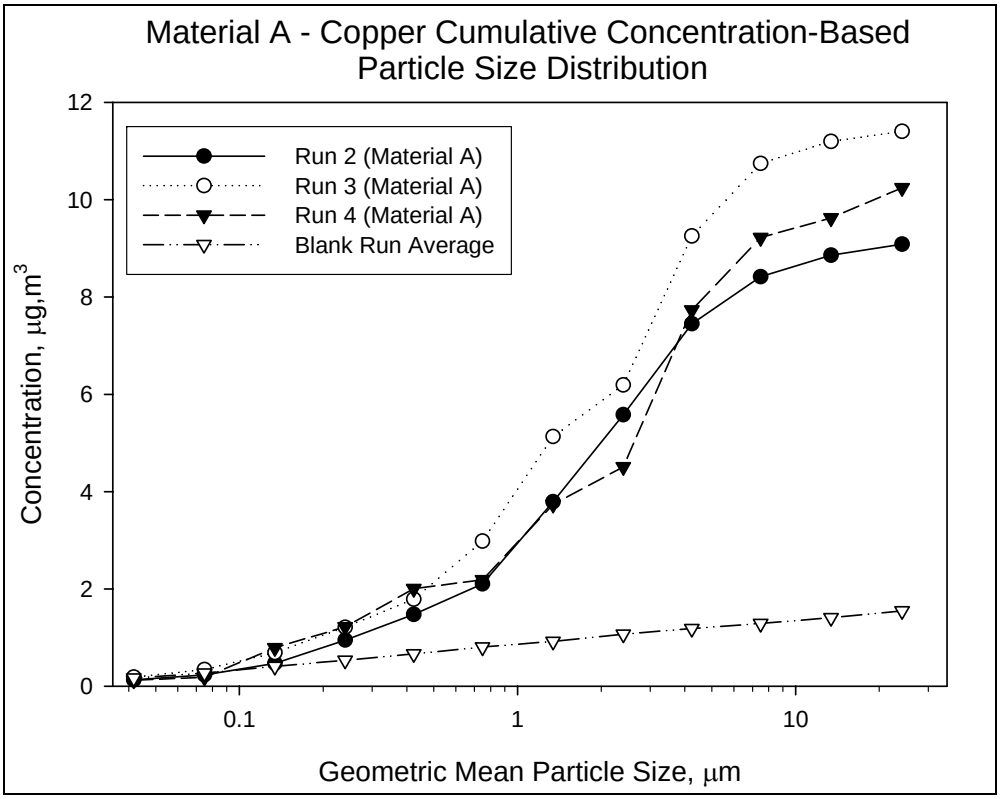

Figure 19: Cumulative Copper Particle Size Distribution for Material A

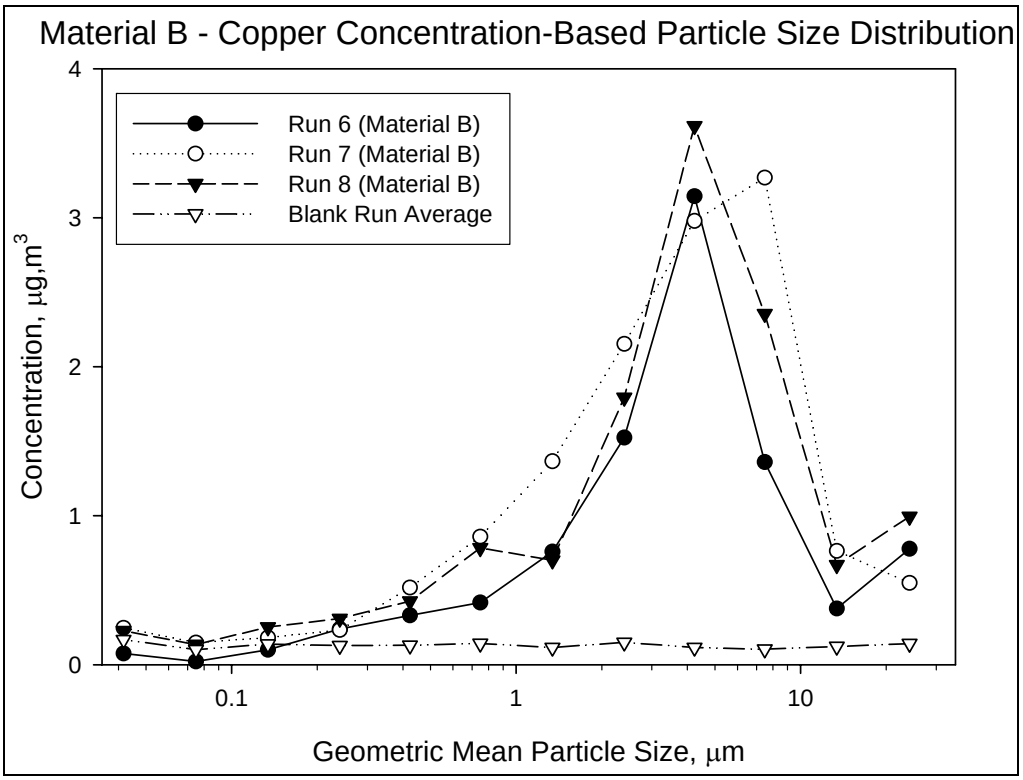

Figure 20: Copper Particle Size Distribution for Material B

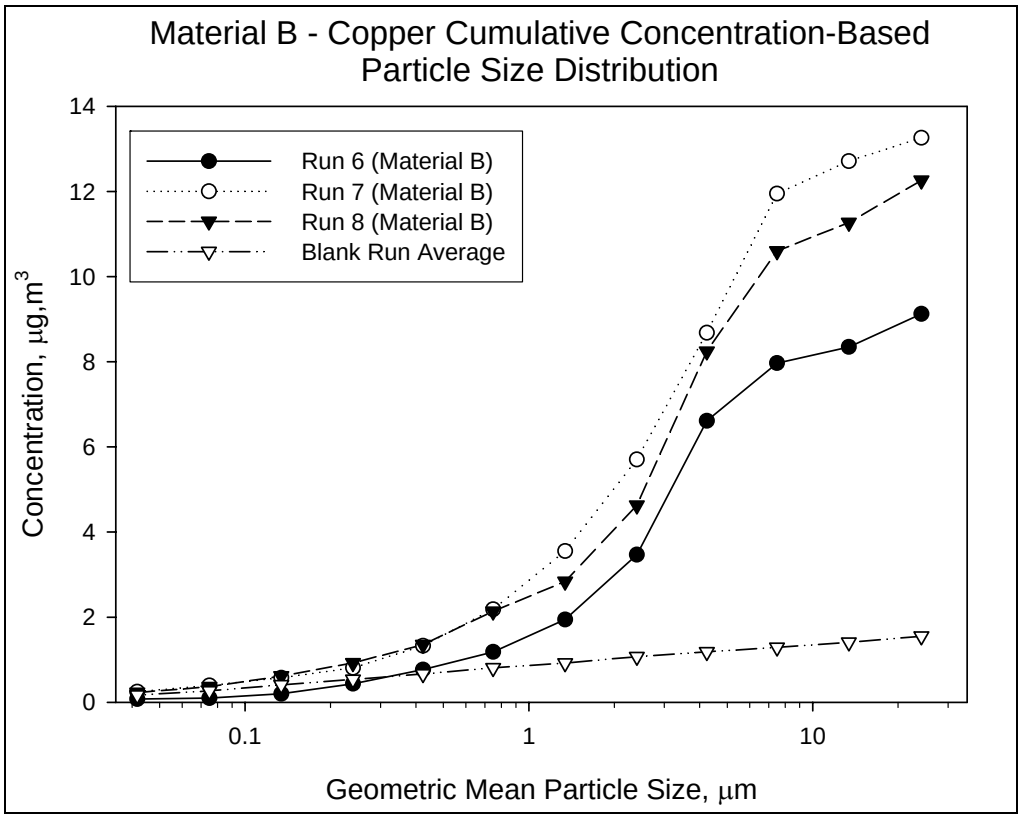

Figure 21: Cumulative Copper Particle Size Distribution for Material B

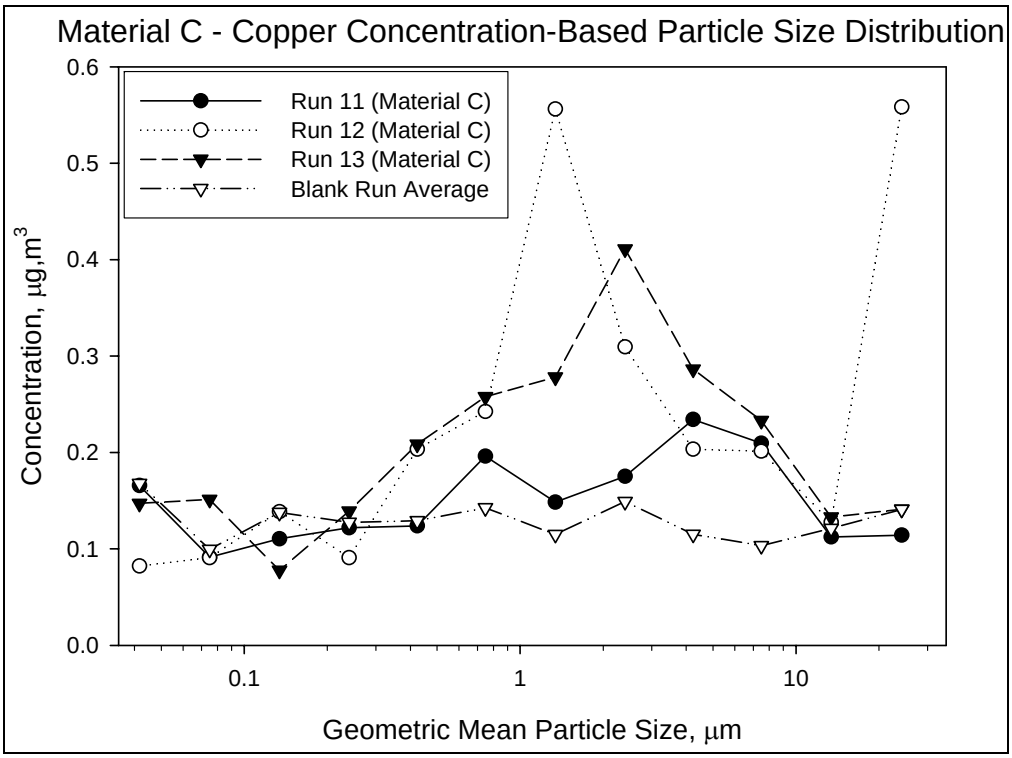

Figure 22: Copper Particle Size Distribution for Material C

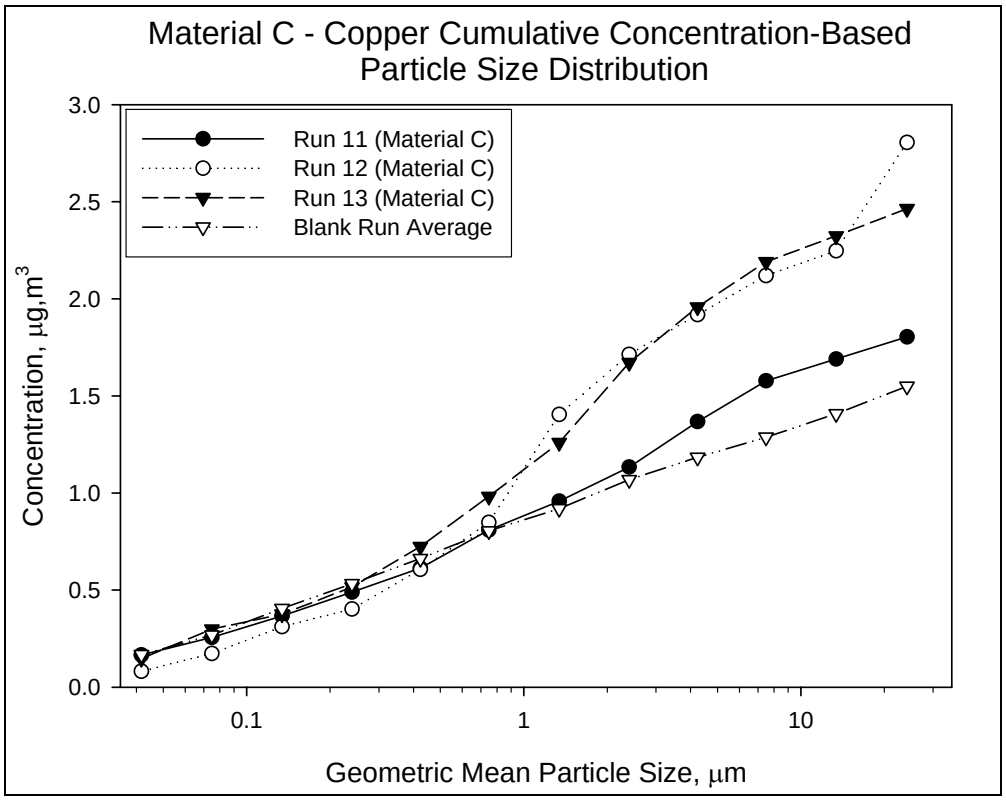

Figure 23: Cumulative Copper Particle Size Distribution for Material C

7b. Calculation of Aerodynamic Particle Size Distributions for the Composite Sample Based on Copper Analysis

Following a procedure analogous to that used for the total mass-based particle size distribution calculations described in Section 6b, the net average Cu concentrations and associated standard errors within each MOUDI size bin were determined for each brake pad material. These values for the individual materials then were used to calculate discrete and cumulative Cu distributions and uncertainties for the hypothetical composite airborne sample using the same 26.4, 14.1, and 59.5% weighting factors for Materials A, B, and C, respectively.

The discrete and cumulative net average Cu distributions and associated uncertainties are shown in Figures 24 and 25, respectively, for Materials A, B, and C. A comparison between Figures 12 and 25 reveals that the Cu content of airborne BPWD particles from Materials A, B, and C was approximately 6.8, 4.7, and 6.3%, respectively, of the overall total mass.

Discrete and cumulative net average Cu distributions and associated uncertainties are shown in Figures 26 and 27, respectively, for the airborne fraction of the representative BPWD sample. Actual copper distribution data are given in Table 2 in Appendix B, and the characteristic values associated with the copper-based composite particle size distribution appropriate for modeling purposes are given in Appendix E.

Comparing Figures 14 and 27 reveals that the Cu content of airborne BPWD particles from the hypothetical representative sample is approximately 6% of the overall total mass. A more rigorous calculation based on the data from Tables 1 and 2 in Appendix B reveals that the copper content of the hypothetical composite airborne sample would be 5.8 ± 0.4 %.

Following the same procedures described in Section 6c, the aerodynamic mass mean diameter for the theoretical composite sample based on copper analysis was calculated to be 4.8 ± 0.4 μm. This value was not statistically different from the previously determined mass mean particle diameter of 5.3 ± 0.2 μm based on total particle mass.

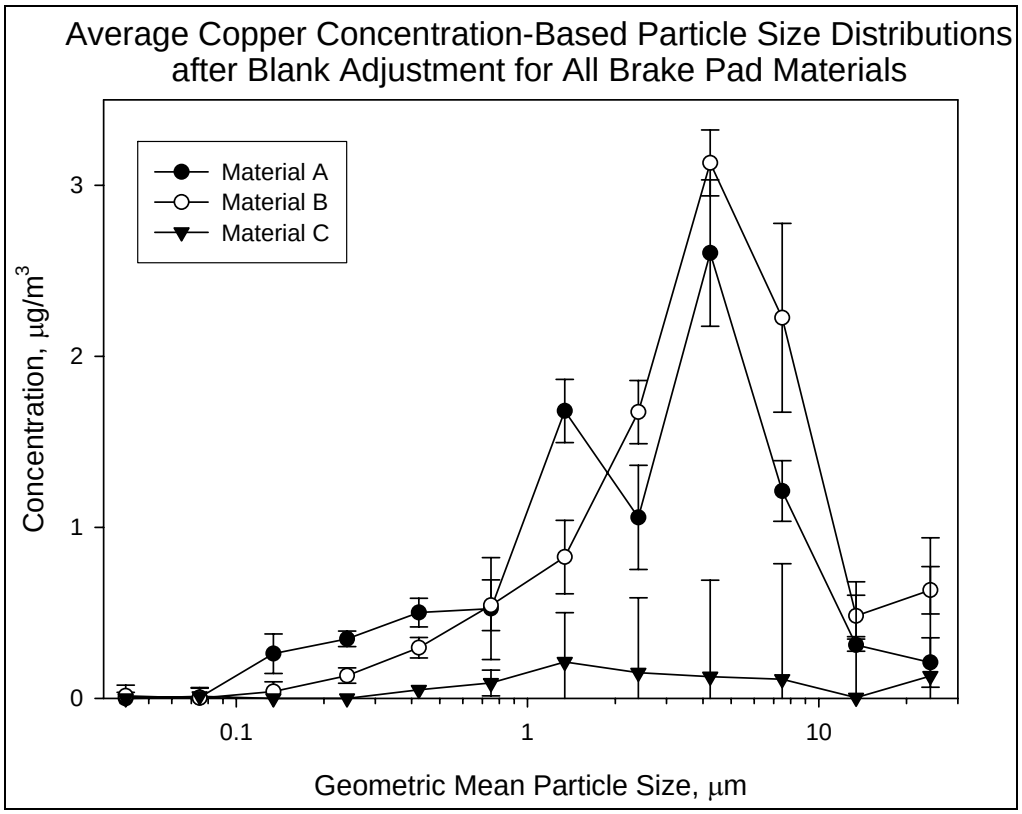

Figure 24: Net Average Copper Particle Size Distributions for Materials A, B, and C

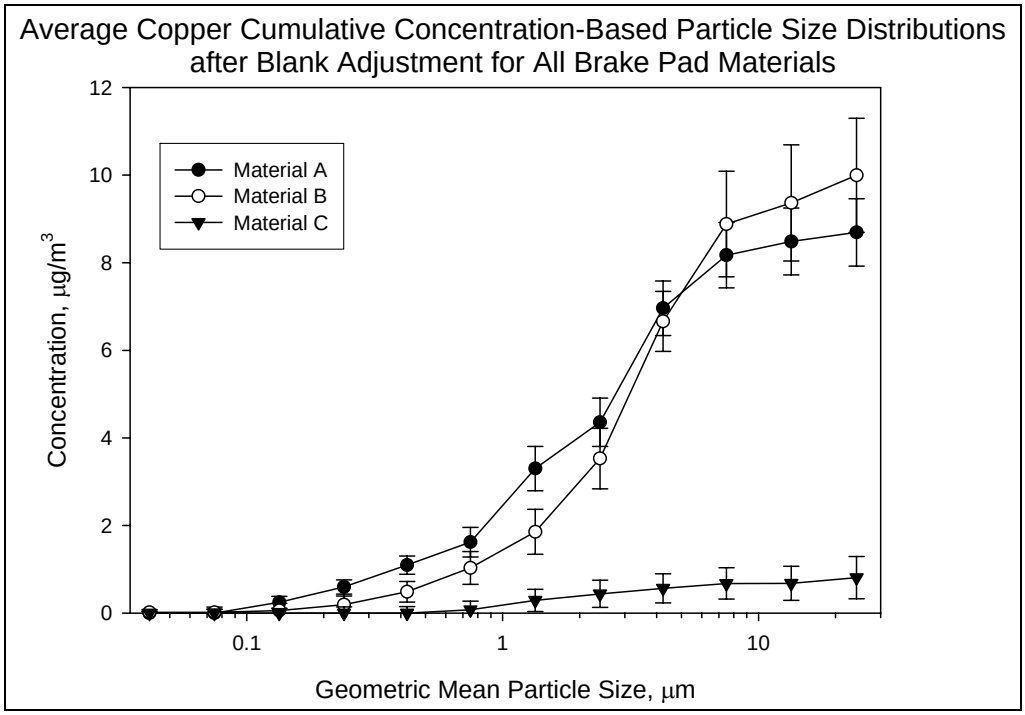

Figure 25: Net Average Cumulative Copper Particle Size Distributions for Materials A, B, and C

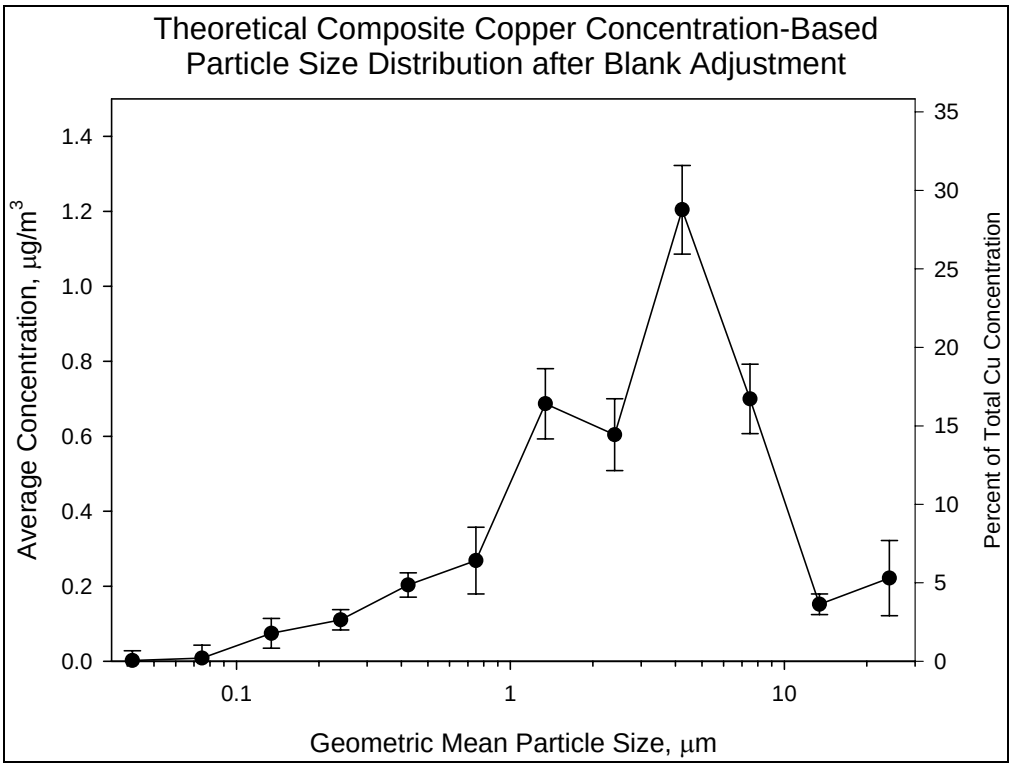

Figure 26: Copper Particle Size Distribution for Hypothetical Composite Material

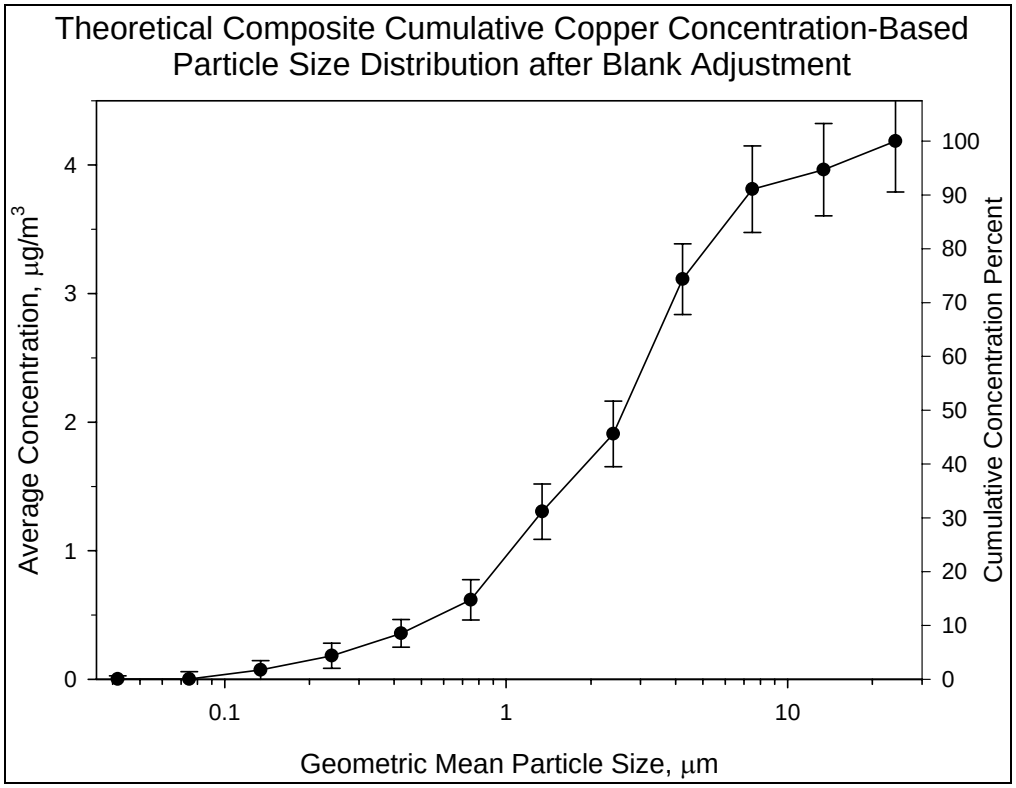

Figure 27: Cumulative Copper Particle Size Distribution for Hypothetical Composite Material

7c. Aerodynamic Particle Size Distributions Based on Iron Analysis

The distributions of Fe for all MOUDI runs are presented in Figure 28. All data used to generate Figure 28 are given in Table 5 of Appendix C. Discrete and cumulative Fe distributions for the blank/background MOUDI runs are shown in Figures 29 and 30, respectively. Consistent with the mass- and Cu-based particle size distribution data, variability was evident in the background Fe measurements. An average background Fe distribution was calculated from the three replicate background measurements, and an average Fe content of 78% was calculated for the background particle concentrations. Discrete and cumulative Fe distributions for Material A relative to the average Fe background are shown in Figures 31 and 32, respectively. Analogous Fe distributions for Materials B and C are presented in Figures 33 and 34 and in Figures 35 and 36, respectively.

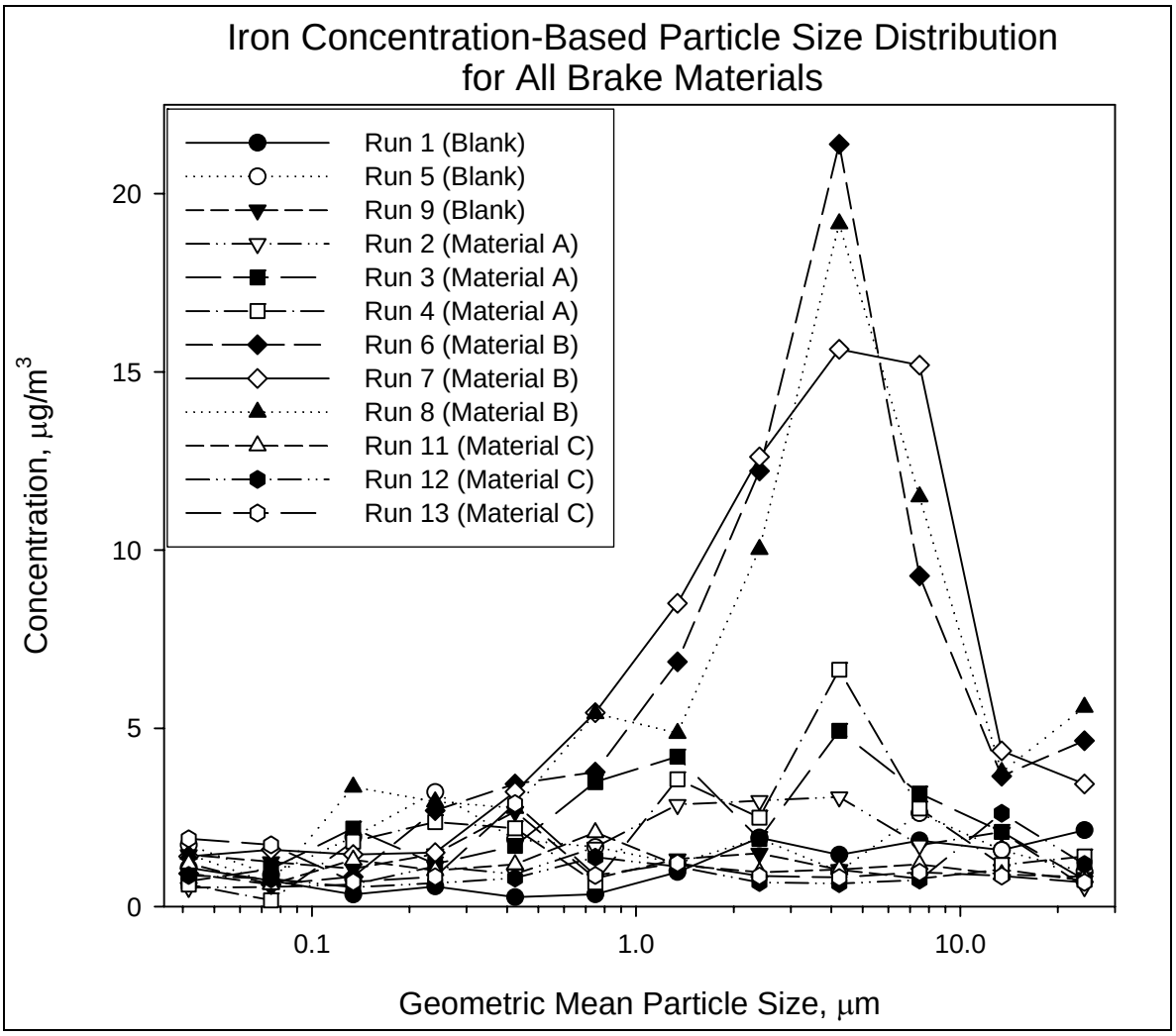

Figure 28: Iron Particle Size Distributions for Materials A, B, and C and Blank Runs

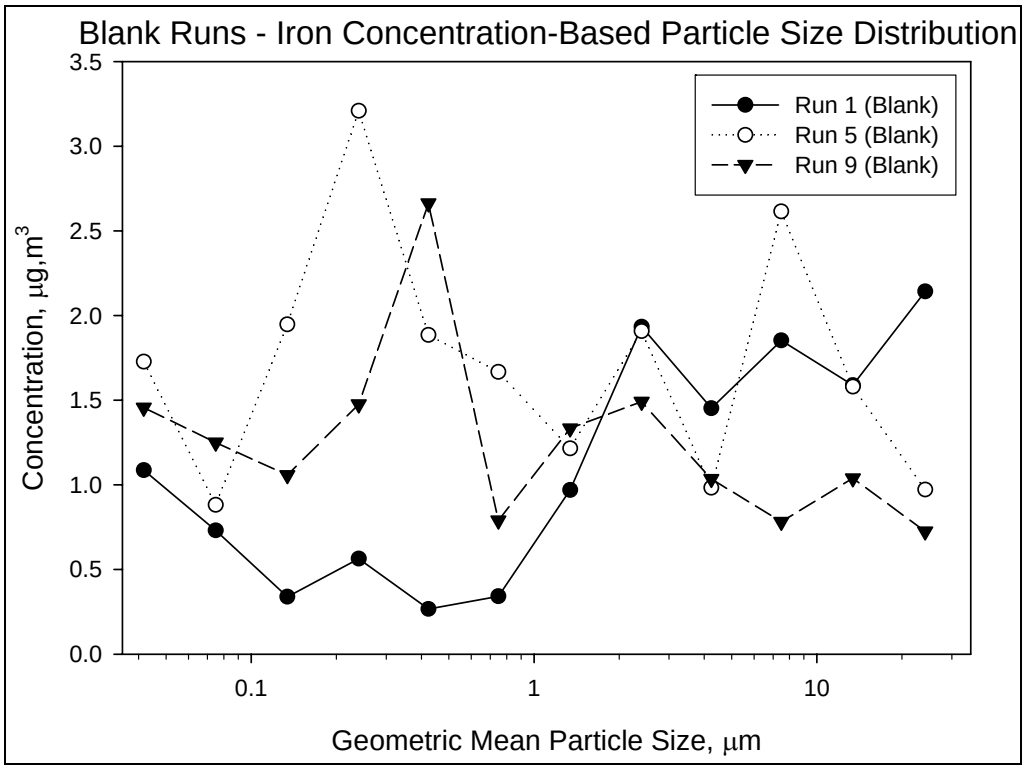

Figure 29: Iron Particle Size Distribution for the Blank Runs

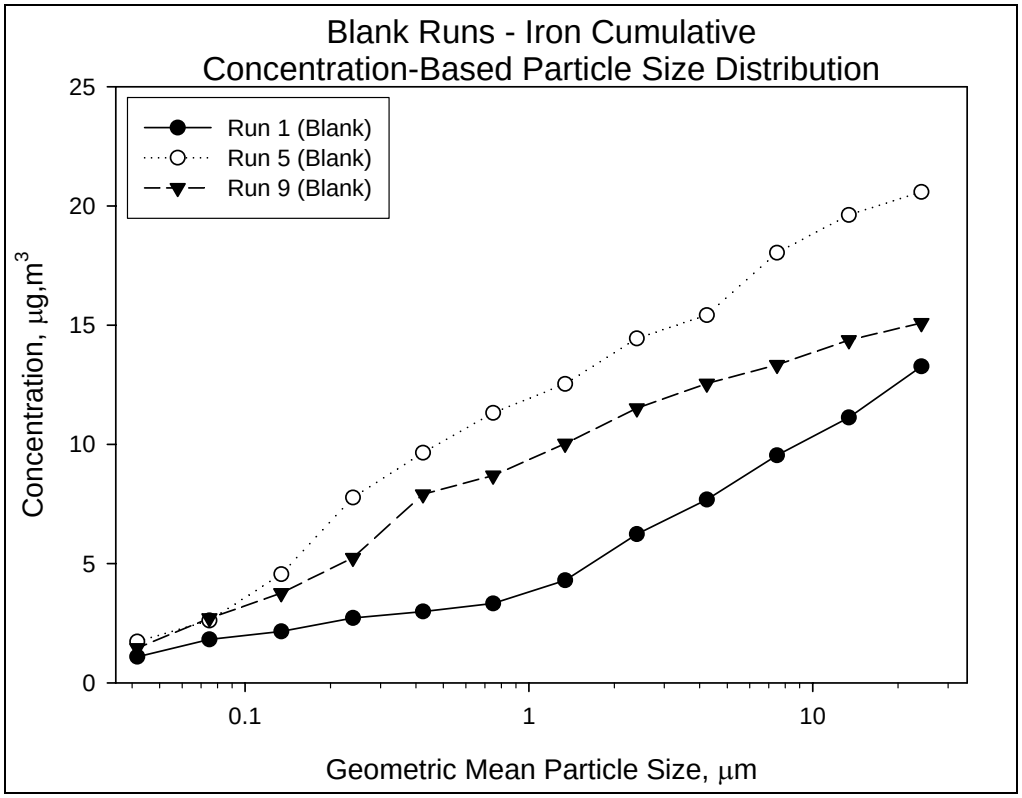

Figure 30: Cumulative Iron Particle Size Distribution for the Blank Runs

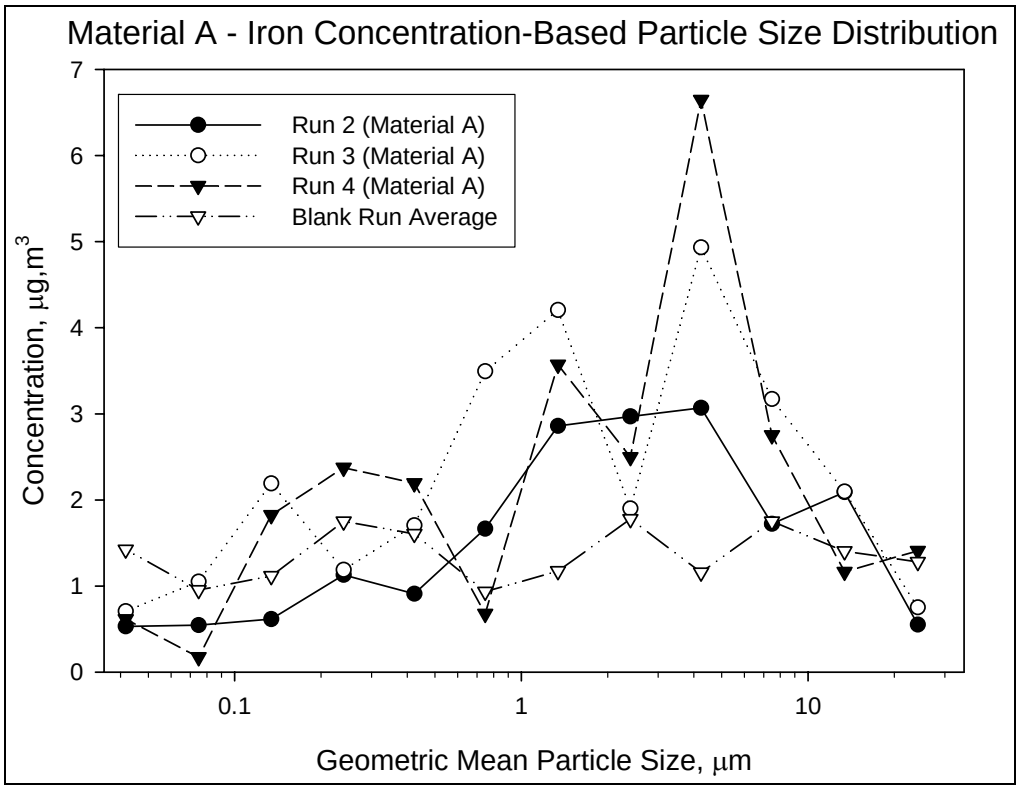

Figure 31: Iron Particle Size Distribution for Material A

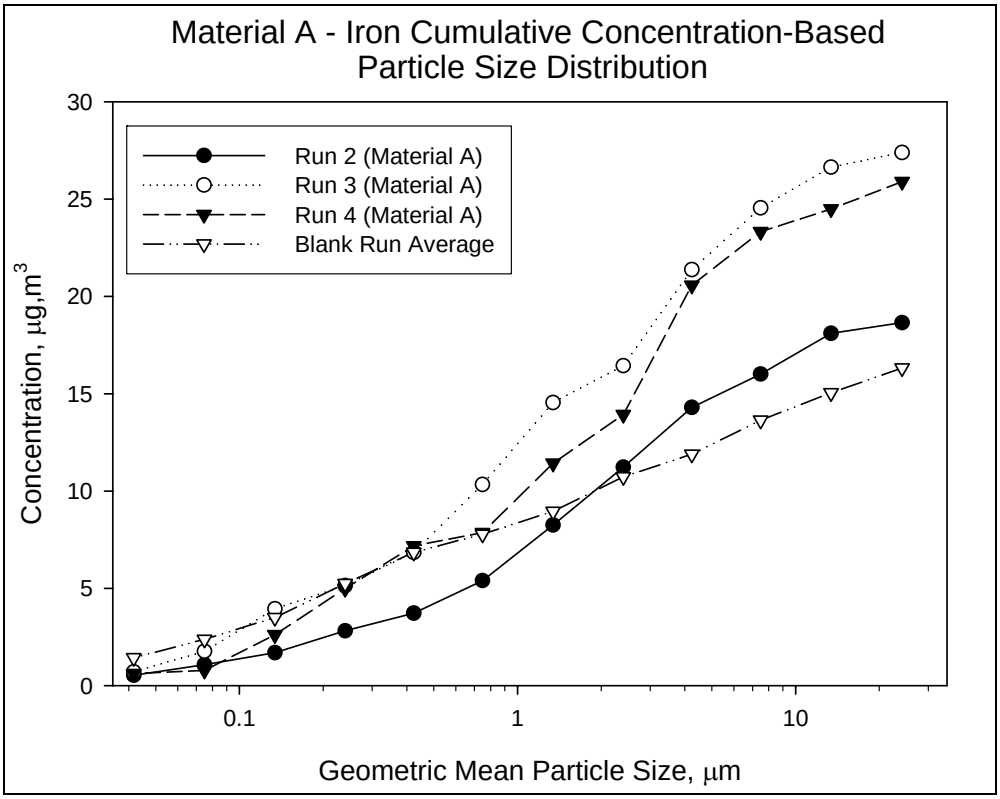

Figure 32: Cumulative Iron Particle Size Distribution for Material A

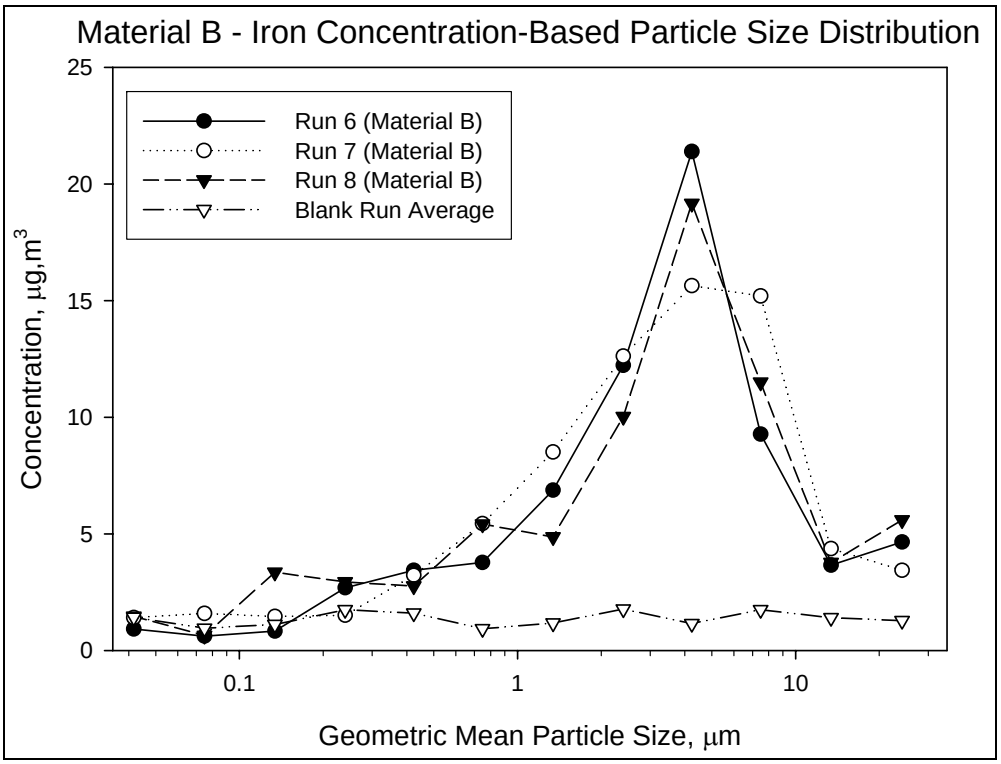

Figure 33: Iron Particle Size Distribution for Material B

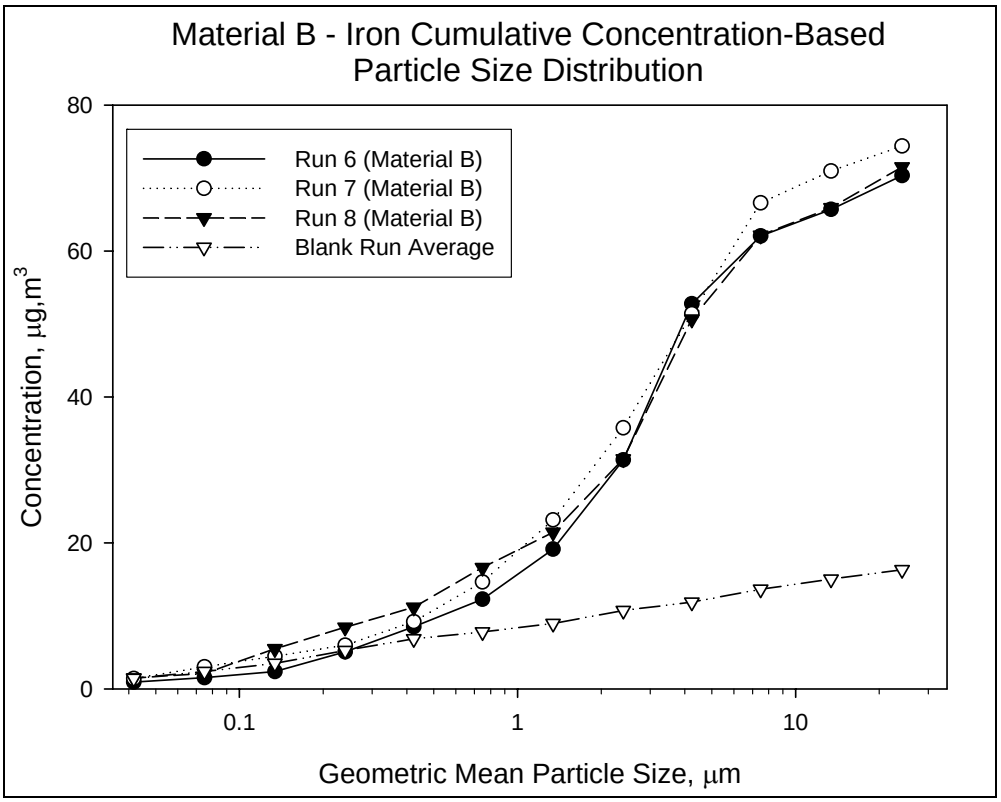

Figure 34: Cumulative Iron Particle Size Distribution for Material B

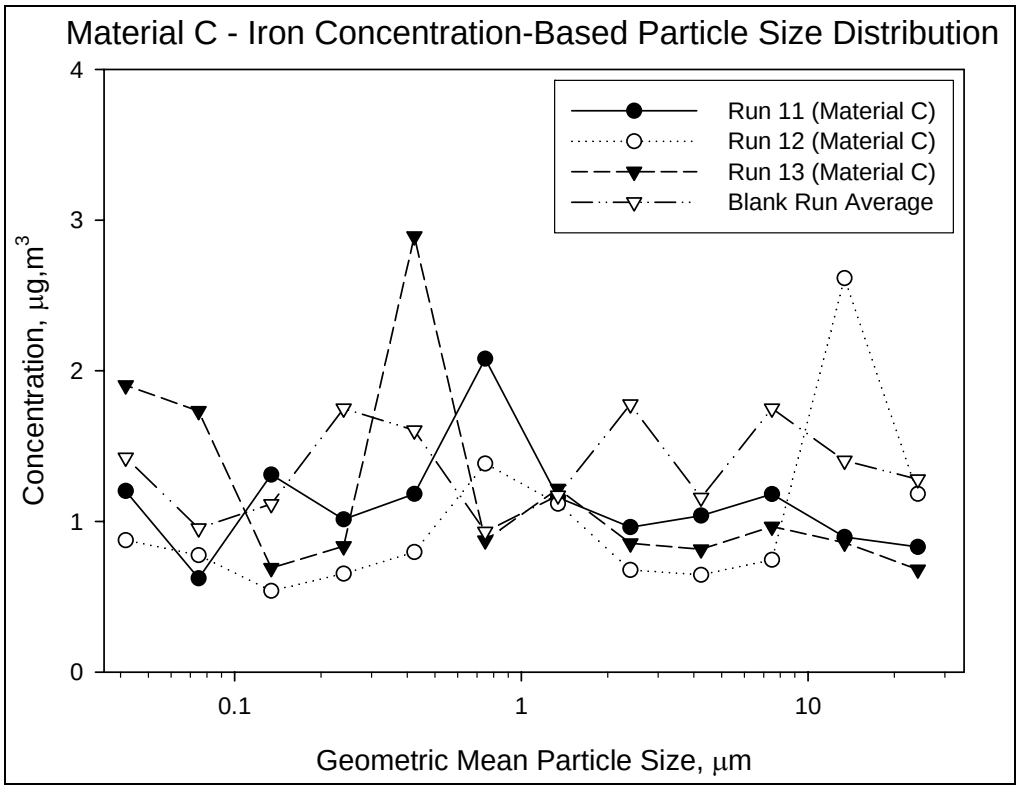

Figure 35: Iron Particle Size Distribution for Material C

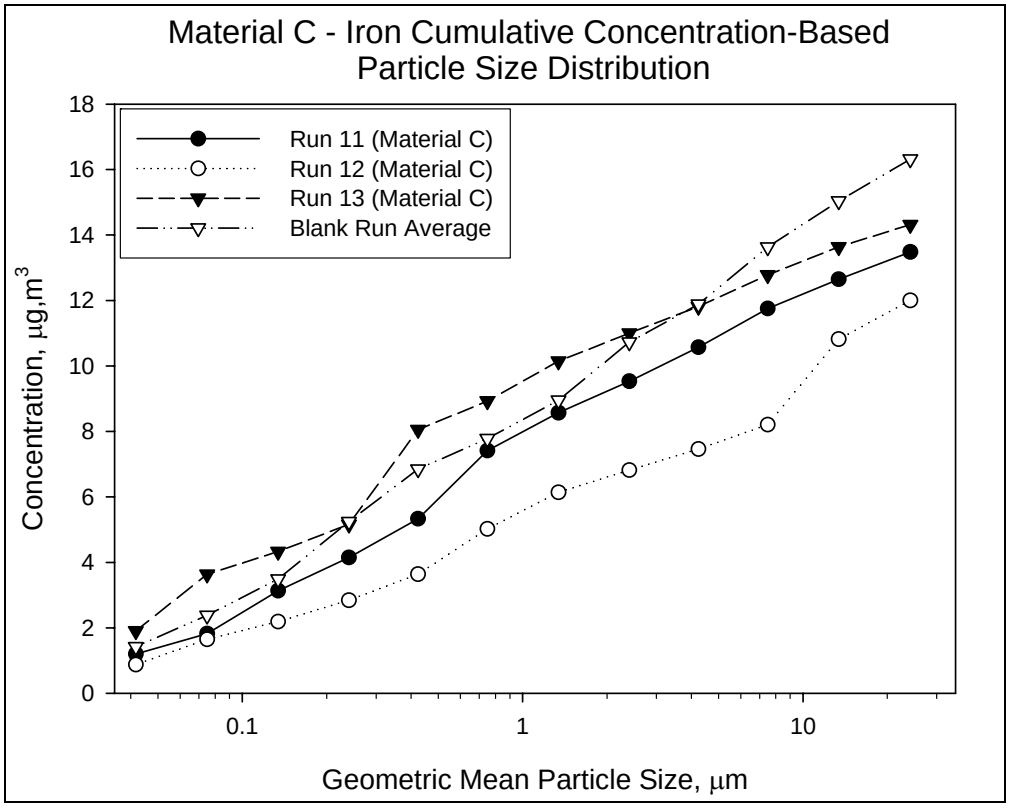

Figure 36: Cumulative Iron Particle Size Distribution for Material C

7d. Calculation of Aerodynamic Particle Size Distributions for the Composite Sample Based on Iron Analysis

Following the procedure described previously, the net average Fe concentrations and associated standard errors within each MOUDI size bin were determined for each brake pad material. These values for the individual materials then were used to calculate discrete and cumulative Fe distributions and uncertainties for the hypothetical composite airborne sample using the same 26.4, 14.1, and 59.5% weighting factors for Materials A, B, and C, respectively.

The discrete and cumulative net average Fe distributions and associated uncertainties are shown in Figures 37 and 38, respectively, for Materials A, B, and C. A comparison between Figures 12 and 38 reveals that the Fe content of airborne BPWD particles from Materials A and B was approximately 6.2 and 26.5%, respectively, of the overall total mass. For Material C, the low generation of airborne BPWD particles combined with the very high Fe signature in the background particles did not permit its Fe content to be calculated.

Discrete and cumulative net average Fe distributions and associated uncertainties are shown in Figures 39 and 40, respectively, for the airborne fraction of the representative BPWD sample. Actual iron distribution data are given in Table 3 in Appendix B, and the characteristic values associated with the iron-based composite particle size distribution appropriate for modeling purposes are given in Appendix E.

Comparing Figures 14 and 40 reveals that the Fe content of airborne BPWD particles from the hypothetical representative sample is approximately 15% of the overall total mass. A more rigorous calculation based on the data from Tables 1 and 3 in Appendix B reveals that the iron content of the hypothetical composite airborne sample would be 14.8 ± 2.0 %.

Following the same procedures described in Section 6c, the aerodynamic mass mean diameter for the theoretical composite sample based on iron analysis was calculated to be 4.8 ± 1.0 μm. This value was not statistically different from the previously determined mass mean particle diameter of 5.3 ± 0.2 μm based on total particle mass.

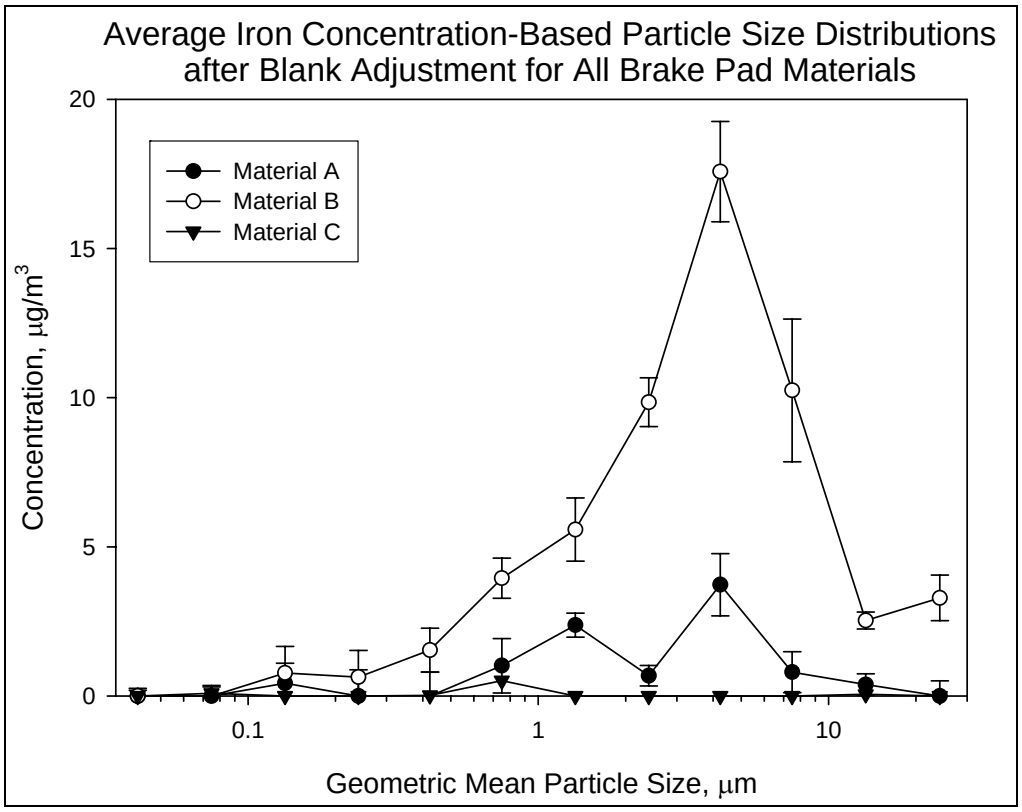

Figure 37: Net Average Iron Particle Size Distributions for Materials A, B, and C

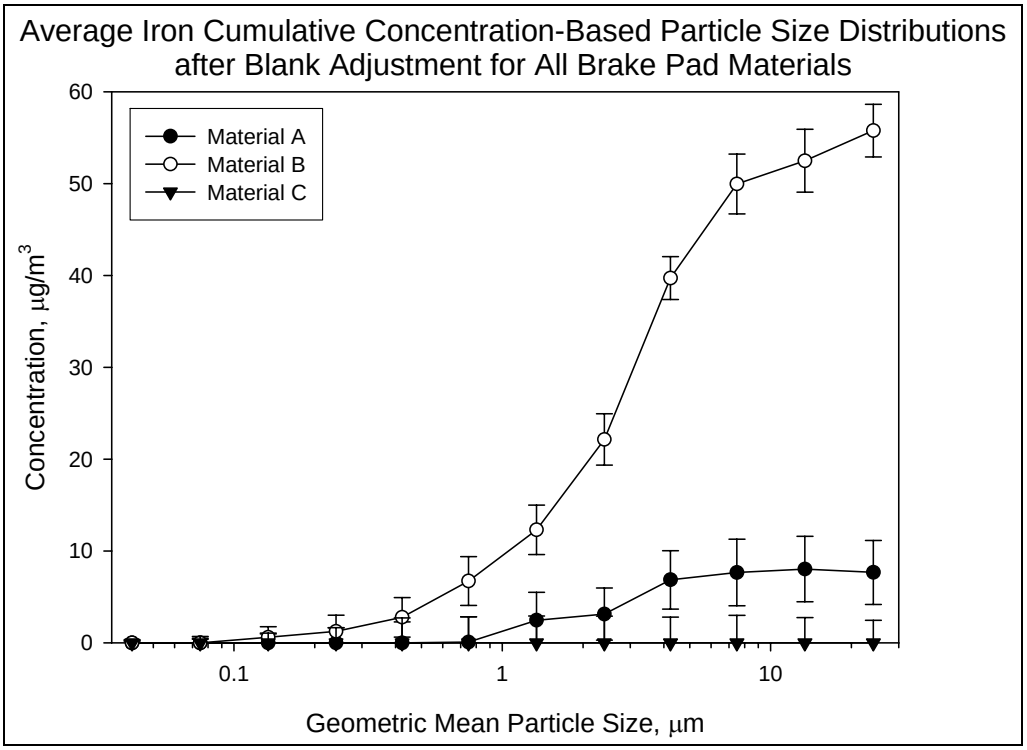

Figure 38: Net Average Cumulative Iron Particle Size Distributions for Materials A, B, and C

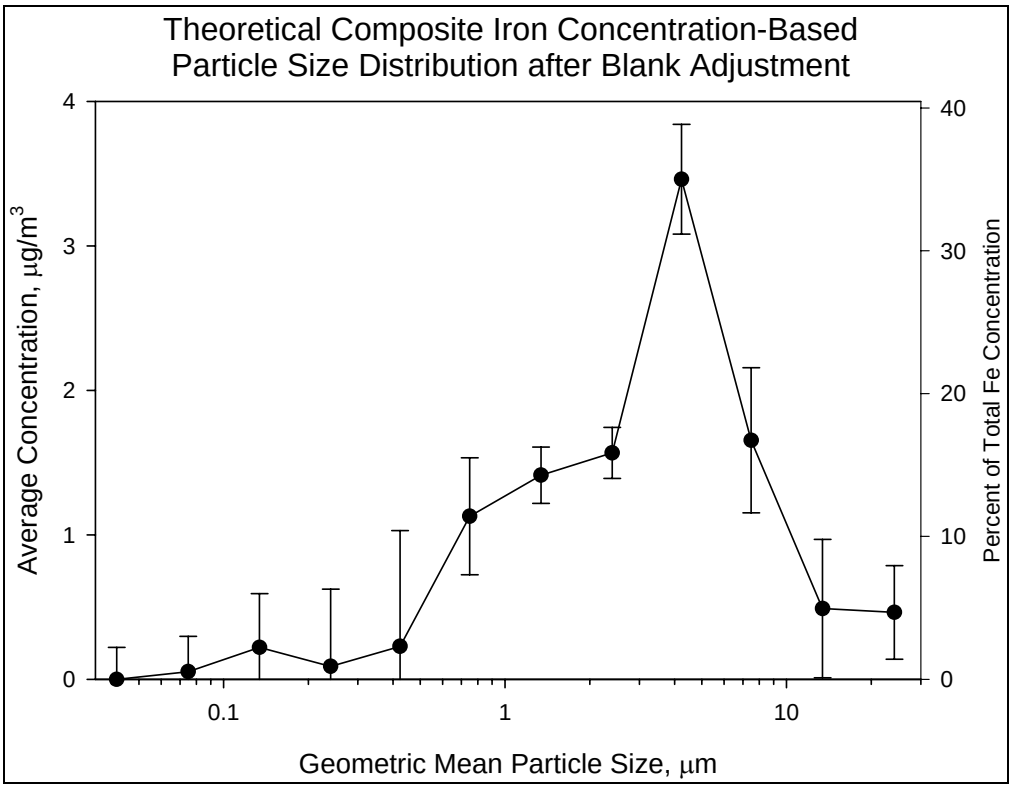

Figure 39: Iron Particle Size Distribution for Hypothetical Composite Material

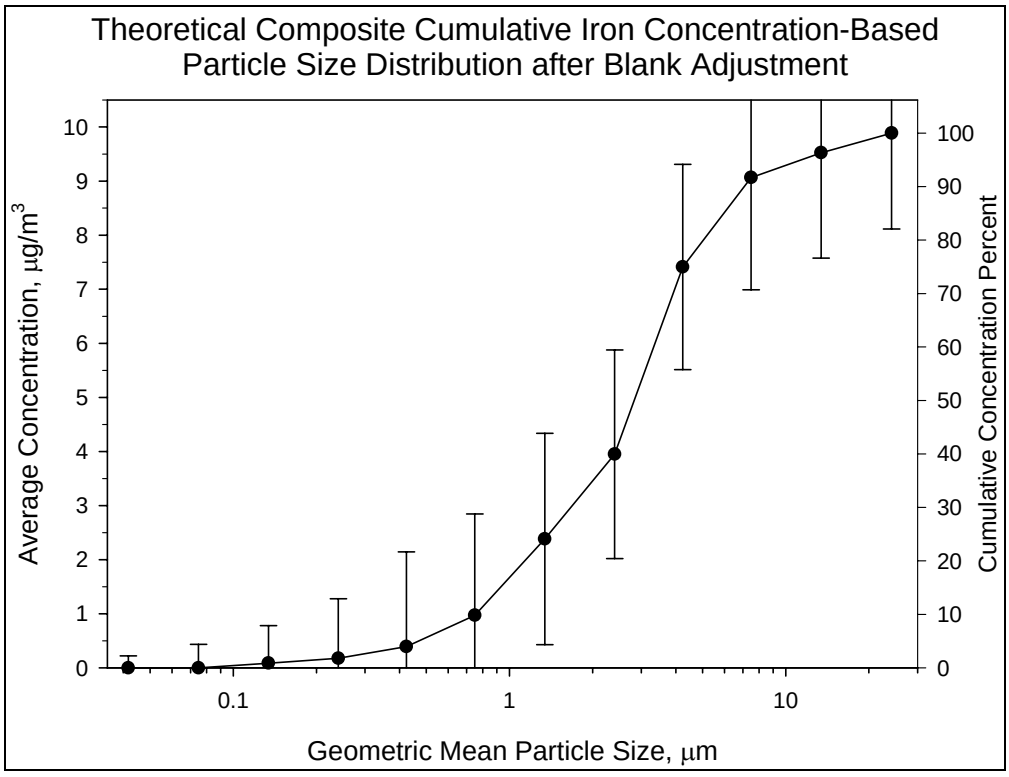

Figure 40: Cumulative Iron Particle Size Distribution for Hypothetical Composite Material

7e. Comparison of Copper, Iron, and Total Airborne Particle Size Distributions for the Theoretical Composite Material

Discrete and cumulative net average distributions and calculated uncertainties for Cu, Fe, and all other particle mass are shown in Figures 41 and 42, respectively, for the airborne fraction of the representative BPWD sample. From Figure 41, in the particle size bins where appreciable amounts of wear debris are seen, Fe is present at greater concentrations than Cu by approximately a factor of 2.5.

Discrete and cumulative particle size distributions based on Cu content and their associated calculated uncertainties are shown in Figure 43 for the airborne fraction of the representative BPWD sample. Figure 44 shows the analogous information for Fe content. Based on these two figures, it appears that no strong trend exists between BPWD particle size and the Cu and Fe contents. The apparent jumps in Cu and Fe contents in the 0.10 to 0.18 μm size bin likely are due to the low total mass accumulation in this size range relative to the high background levels. The numeric data used to create Figures 43 and 44 are shown in Table 4 in Appendix B.

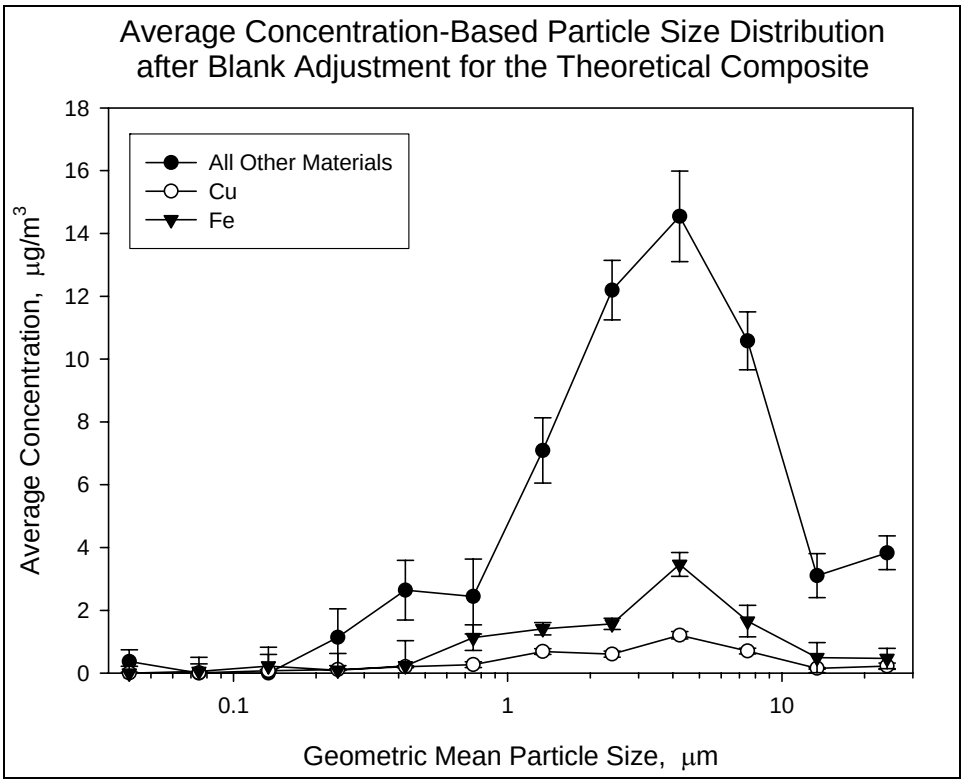

Figure 41: Particle Size Distribution for Components of the Hypothetical Composite Material

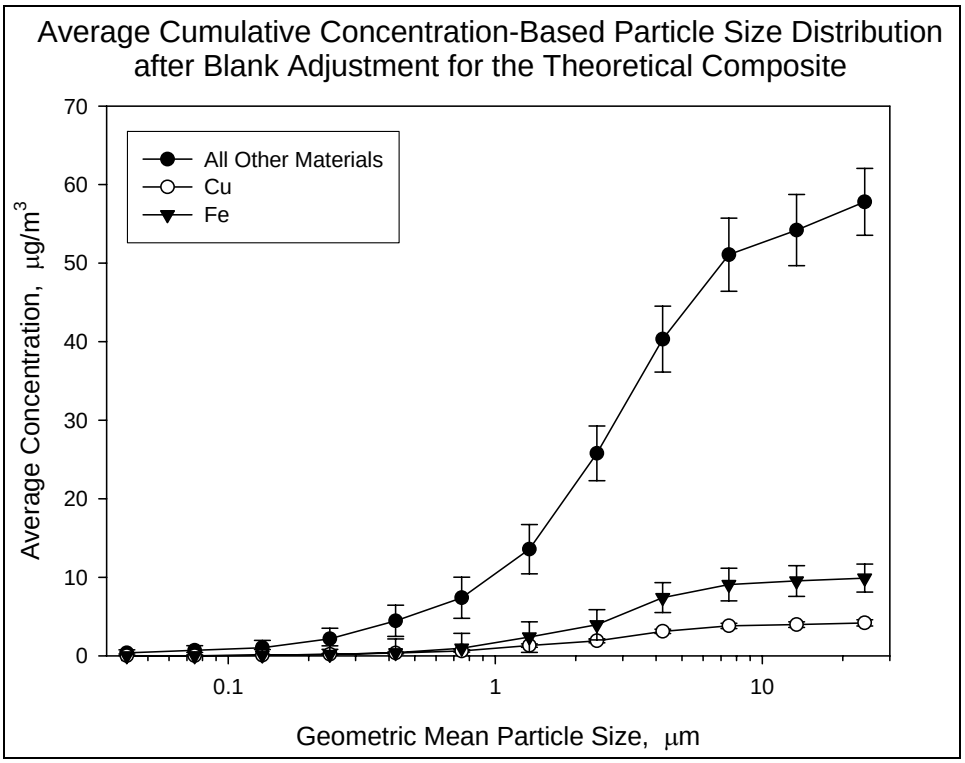

Figure 42: Cumulative Particle Size Distribution for Components of the Hypothetical Composite Material

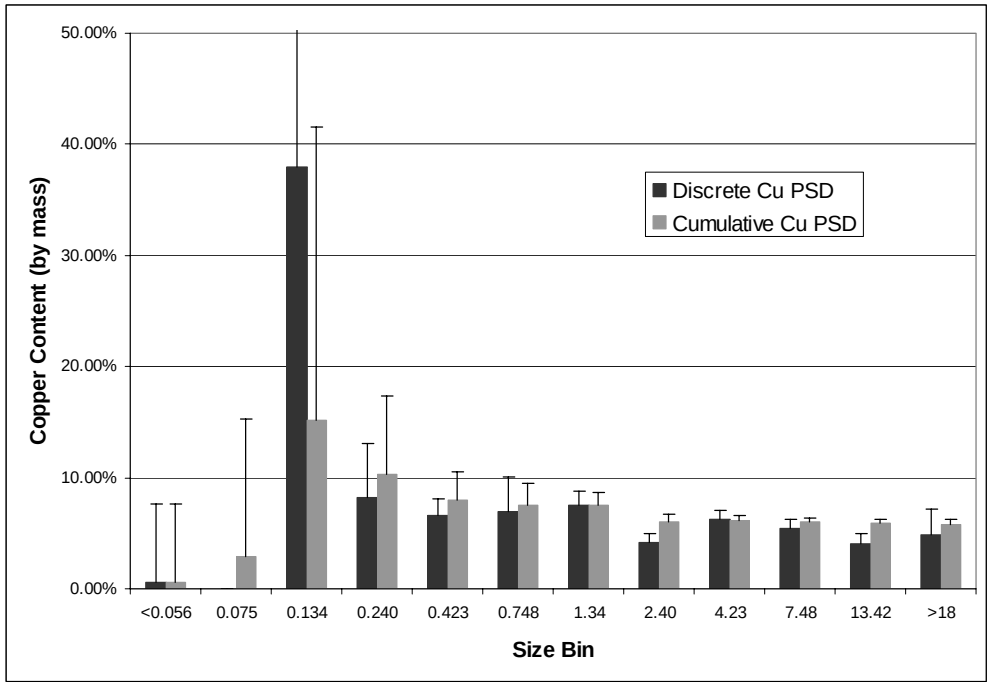

Figure 43: Discrete and Cumulative Particle Size Distributions Based on Copper Content for Theoretical Composite Material

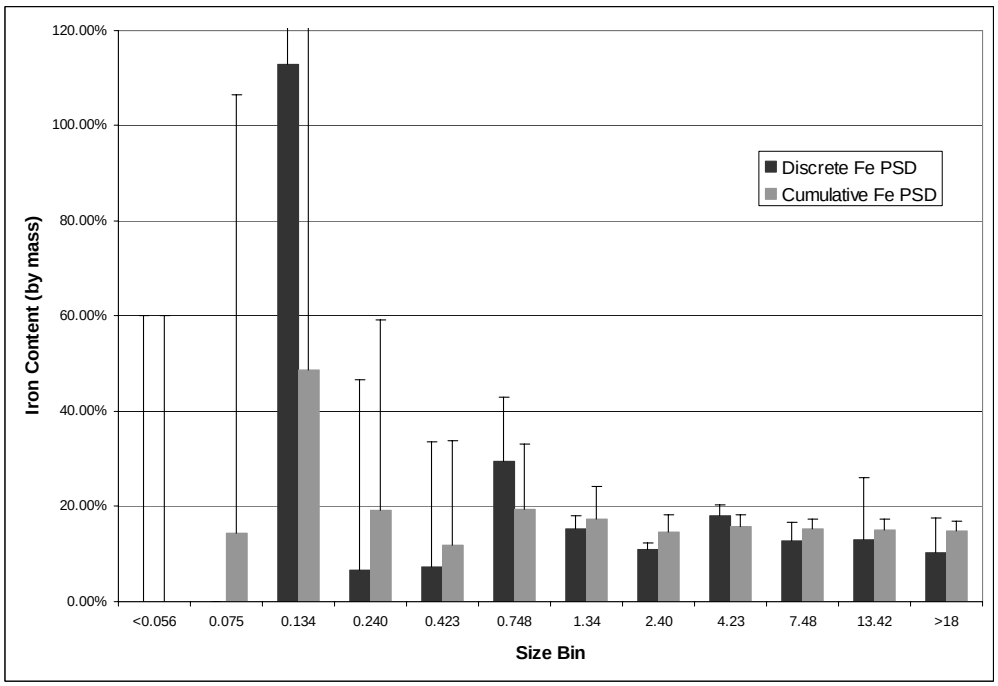

Figure 44: Discrete and Cumulative Particle Size Distributions Based on Iron Content for Theoretical Composite Material

Appendix A: Figures and Drawings from Previous Dynamometer Setup

(from: J. Trainor, T. Duncan, and R. Mangan, *Disc Brake Wear Debris Generation and Collection*, 2002-01-2595, SAE Technical Paper Series, SAE International, Warrendale, PA, 2002)

Figure 1. Brake Dynamometer Components Schematics

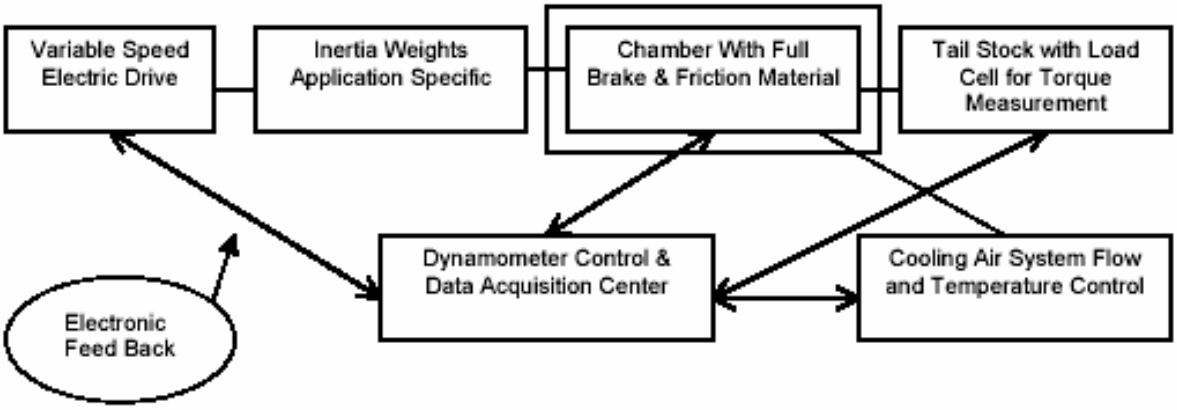

Figure 2. Brake Dynamometer Photograph

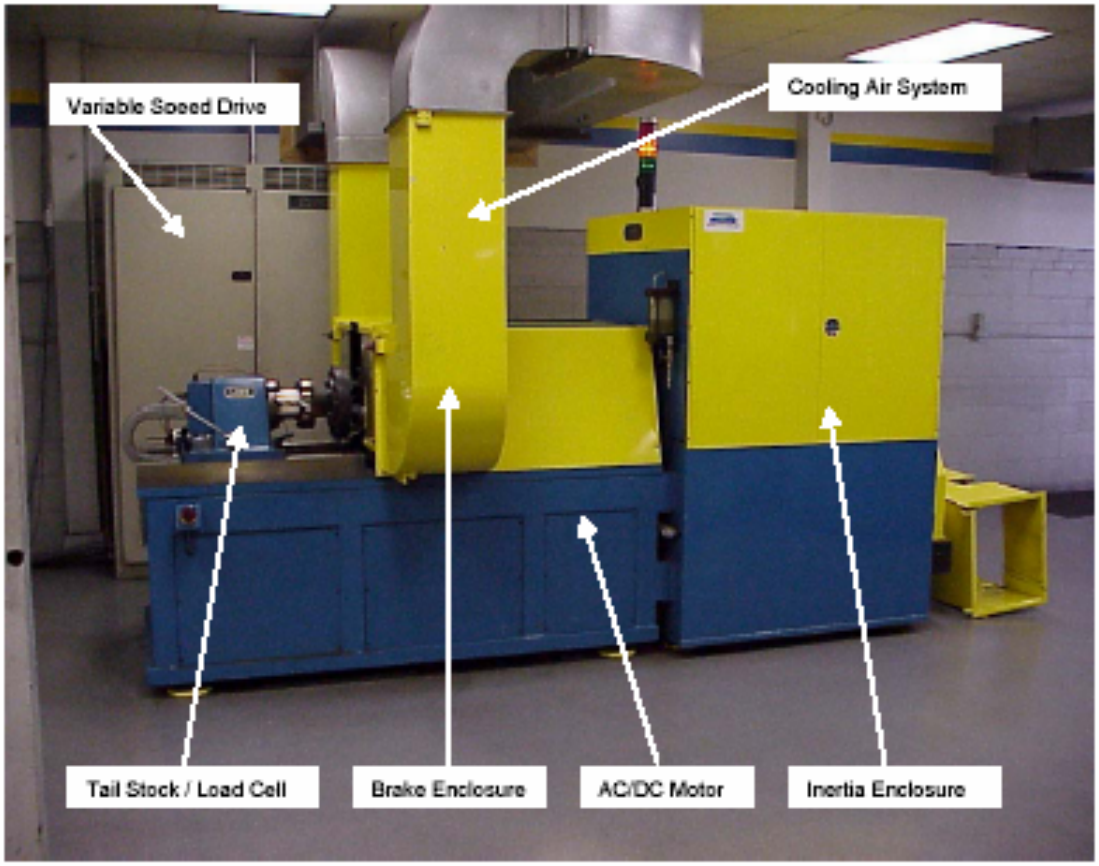

Figure 3. Wear Debris Collection Apparatus Schematic

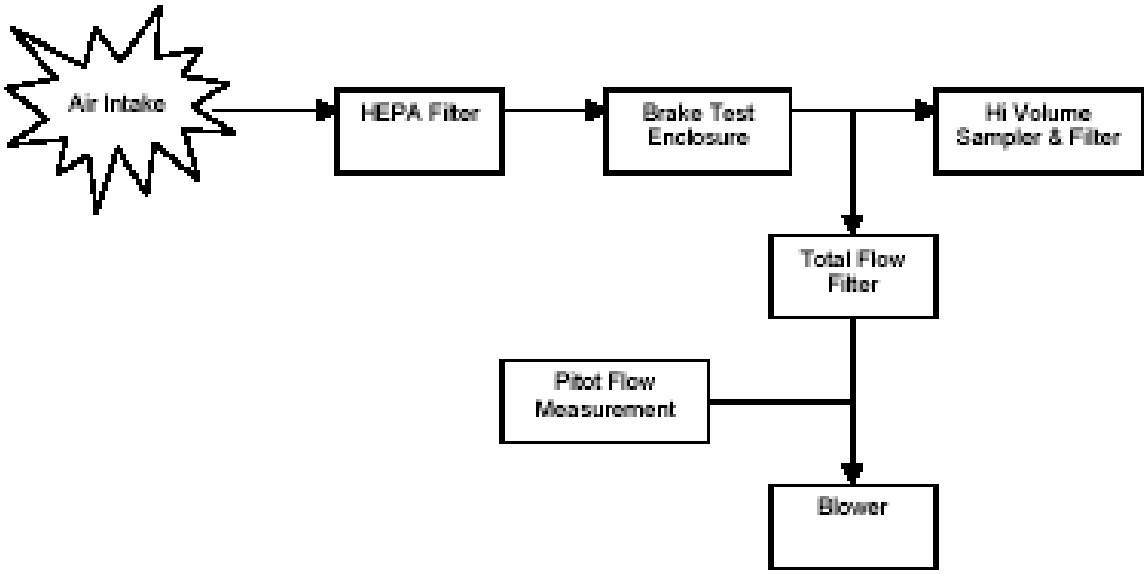

Figure 4. Wear Debris Collection Apparatus Photo

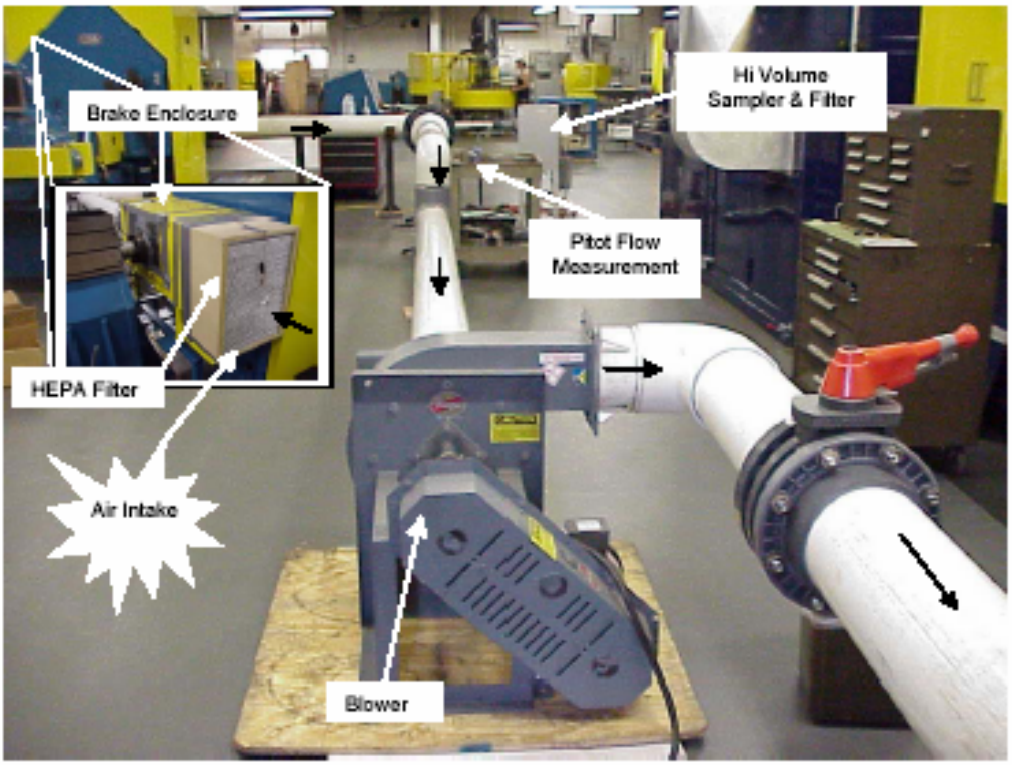

Appendix I. Wear Debris Collection Apparatus and Supplies

Appendix I. a. Piping Arrangement and Required Duct Dimensions for Sample Collection

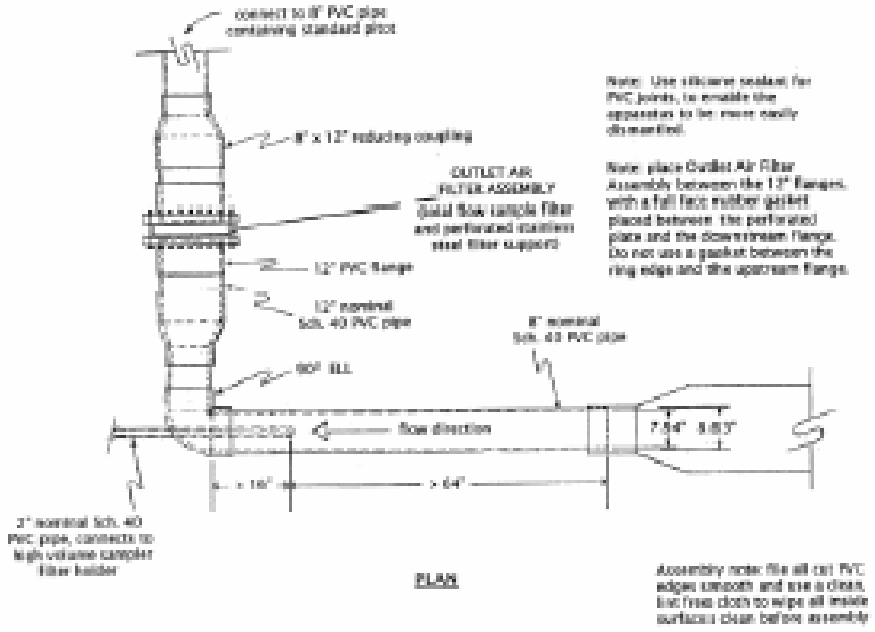

Appendix I. e. Air Sampling Apparatus

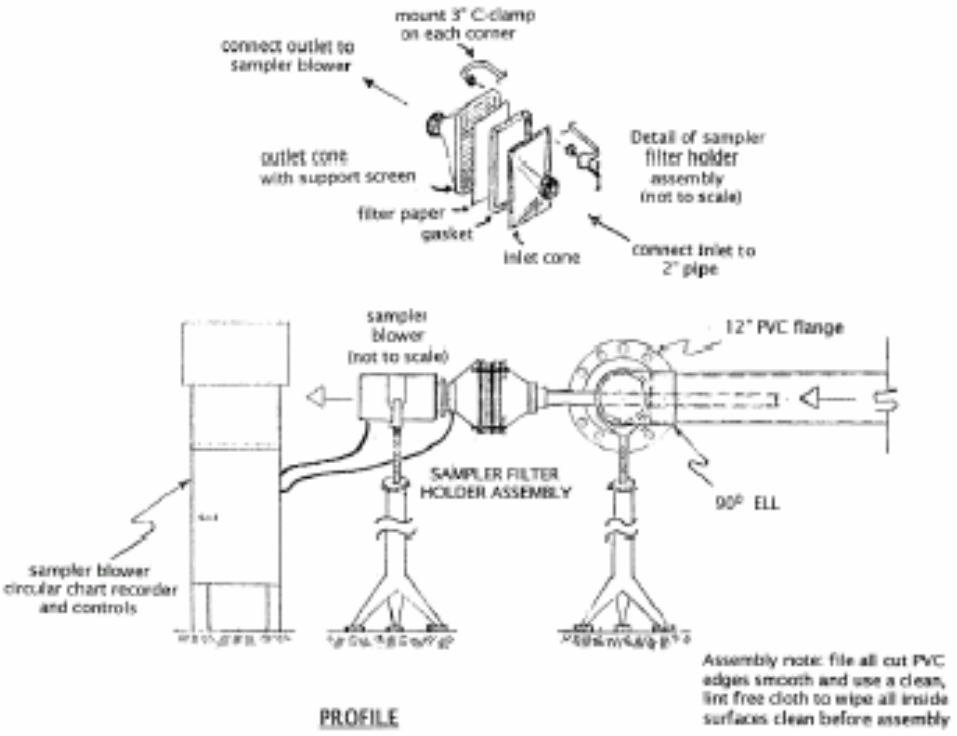

Appendix B: Particle Size Distribution Data

Table 1: Particle Size Distribution Data for the Theoretical Composite Material

Particle Size Bin (µm)	Average Net Concentration (µg/m³)	Average Mass per 2.5 Hours (µg)	Percent Total Concentration (%)
> 18.0	4.52	20.32	6.20
10.0 - 18.0	3.75	16.86	5.15
5.60 - 10.0	12.94	58.21	17.77
3.20 - 5.60	19.21	86.46	26.40
1.80 - 3.20	14.37	64.66	19.74
1.00 - 1.80	9.19	41.36	12.63
0.56 - 1.00	3.84	17.27	5.27
0.32 - 0.56	3.07	13.82	4.22
0.18 - 0.32	1.34	6.04	1.84
0.10 - 0.18	0.20	0.88	0.27
0.056 - 0.10	0.00	0.00	0.00
< 0.056	0.37	1.65	0.50

Table 2: Copper Distribution Data for the Theoretical Composite Material

Particle Size Bin (µm)	Average Net Cu Concentration (µg/m³)	Average Cu Mass per 2.5 Hours (µg)	Percent Total Cu Concentration (%)
> 18.0	0.22	1.00	5.23
10.0 - 18.0	0.15	0.68	3.58
5.60 - 10.0	0.70	3.15	16.50
3.20 - 5.60	1.20	5.42	28.40
1.80 - 3.20	0.60	2.72	14.25
1.00 - 1.80	0.69	3.09	16.19
0.56 - 1.00	0.27	1.21	6.33
0.32 - 0.56	0.20	0.92	4.80
0.18 - 0.32	0.11	0.50	2.61
0.10 - 0.18	0.07	0.34	1.76
0.056 - 0.10	0.01	0.04	0.20
< 0.056	0.00	0.01	0.05

Table 3: Iron Distribution Data for the Theoretical Composite Material

Particle Size Bin (µm)	Average Net Fe Concentration (µg/m³)	Average Fe Mass per 2.5 Hours (µg)	Percent Total Fe Concentration (%)
> 18.0	0.46	2.08	4.30
10.0 - 18.0	0.49	2.20	4.55
5.60 - 10.0	1.65	7.45	15.36
3.20 - 5.60	3.46	15.58	32.14
1.80 - 3.20	1.57	7.05	14.55
1.00 - 1.80	1.41	6.36	13.12
0.56 - 1.00	1.13	5.08	10.48
0.32 - 0.56	0.23	1.02	2.11
0.18 - 0.32	0.09	0.40	0.83
0.10 - 0.18	0.22	1.00	2.06
0.056 - 0.10	0.05	0.24	0.49
< 0.056	0.00	0.00	0.00

Table 4: Copper and Iron Contents in the Theoretical Composite Material

Particle Size Bin (µm)	Mass % Cu	Mass % Fe	Particle Size Range (µm)	Mass % Cu	Mass % Fe
> 18.0	4.91	10.25	ALL	5.82	14.80
10.0 - 18.0	4.05	13.07	< 18.0	5.88	15.10
5.60 - 10.0	5.41	12.79	< 10.0	5.99	15.21
3.20 - 5.60	6.27	18.02	< 5.60	6.13	15.82
1.80 - 3.20	4.21	10.91	< 3.20	6.05	14.52
1.00 - 1.80	7.47	15.37	< 1.80	7.52	17.40
0.56 - 1.00	6.99	29.41	< 1.00	7.57	19.51
0.32 - 0.56	6.62	7.41	< 0.56	8.02	11.88
0.18 - 0.32	8.24	6.65	< 0.32	10.27	19.09
0.10 - 0.18	38.02	112.91	< 0.18	15.11	48.70
0.056 - 0.10	n.a.	n.a.	< 0.10	2.88	14.42
< 0.056	0.57	0.00	< 0.056	0.57	0.00

n.a.: not applicable. Calculation divides by zero.

Appendix C: Filter Weights

Table 5: Material A Filter Weights

Run #1 - Blank 1 (Run Time = 2.00 hours)

MOUDI Position	Filter Number	Initial Weight (µg)	Final Weight (µg)
1	050304025	168660.8	168669.1
2	050304024	169995.9	169999.8
3	050304023	160320.9	160322.1
4	050304022	173274.1	173280.6
5	050304021	164654.4	164659.5
6	050304020	160337.2	160341.3
7	050304019	156857.7	156870.8
8	050304018	162472.8	162480.8
9	050304017	157417.5	157424.9
10	050304016	154726.2	154738.6
11	050304015	167980.7	167979.3
12	062404401	106014.6	106019.2

Run #2 - Material A (Run Time = 2.55 hours)

MOUDI Position	Filter Number	Initial Weight (µg)	Final Weight (µg)
1	050304036	151545.6	151596.6
2	050304035	162899.6	162919.0
3	050304034	162492.9	162554.7
4	050304033	165916.9	166017.5
5	050304032	167215.9	167313.9
6	050304031	160535.5	160615.6
7	050304030	159600.6	159659.8
8	050304029	156335.0	156374.7
9	050304028	156336.8	156366.8
10	050304027	150574.4	150588.4
11	050304026	149736.4	149743.6
12	063404402	104193.0	104204.8

Run #3 - Material A (Run Time = 2.48 hours)

Filter Number	Initial Weight (µg)	Final Weight (µg)
050304047	166794.1	166834.1
050304046	157649.3	157676.2
050304045	163998.2	164092.8
050304044	165417.3	165581.9
050304043	156173.4	156311.3
050304042	163206.1	163316.7
050304041	168968.5	169026.7
050304040	171888.0	171928.0
050304039	167200.1	167221.6
050304038	171071.1	171079.0
050304037	163294.6	163315.7
062404403	102691.1	102692.4

Run #4 - Material A (Run Time = 2.55 hours)

Filter Number	Initial Weight (µg)	Final Weight (µg)
050404059	154002.9	154044.6
050404058	157629.1	157660.6
050404057	159052.9	159137.7
050404056	160450.5	160623.3
050404055	158137.1	158280.8
050404054	156048.8	156132.8
050404053	149712.9	149766.3
050404051	152401.3	152441.8
050304050	169666.3	169692.6
050304049	170953.8	170963.1
050304048	167662.4	167666.8
062404404	100643.2	100658.2

Table 6: Material B Filter Weights

Run #5 - Blank 2 (Run Time = 1.92 hours)

MOUDI Position	Filter Number	Initial Weight (µg)	Final Weight (µg)
1	050404070	168487.8	168498.7
2	050404069	171143.3	171151.5
3	050404068	167552.6	167549.2
4	050404067	169888.7	169891.8
5	050404066	169574.4	169577.2
6	050404065	160947.3	160951.9
7	050404064	163773.3	163777.7
8	050404063	167174.3	167178.4
9	050404062	166473.9	166479.6
10	050404061	162643.8	162648.3
11	050404060	163707.5	163715.6
12	062404405	101866.7	101869.1

Run #6 - Material B (Run Time = 2.57 hours)

MOUDI Position	Filter Number	Initial Weight (µg)	Final Weight (µg)
1	050604081	148074.1	148167.7
2	050604080	155500.8	155586.9
3	050604079	149644.0	149858.8
4	050604078	145634.7	145914.0
5	050604077	154619.3	154792.5
6	050604076	151168.3	151259.6
7	050404075	168446.2	168508.0
8	050404074	164312.2	164348.0
9	050404073	154314.8	154341.3
10	050404072	161881.8	161896.0
11	050404071	172151.6	172156.5
12	062404406	100224.4	100236.6

Run #7 - Material B (Run Time = 2.48 hours)

Filter Number	Initial Weight (µg)	Final Weight (µg)
050604092	155171.2	155254.4
050604091	146624.2	146705.0
050604090	150982.3	151219.3
050604089	153487.5	153766.9
050604088	150184.4	150336.5
050604087	150050.3	150141.7
050604086	154606.7	154662.6
050604085	143090.8	143140.4
050604084	145979.2	146009.9
050604083	150081.2	150105.5
050604082	149050.4	149057.6
062404407	98107.6	98111.5

Run #8 - Material B (Run Time = 2.52 hours)

Filter Number	Initial Weight (µg)	Final Weight (µg)
051004103	163170.6	163285.2
051004102	168222.6	168326.7
051004101	158286.8	158492.9
050604100	153081.8	153343.6
050604099	151345.3	151489.7
050604098	153217.6	153260.3
050604097	147488.8	147543.0
050604096	151092.9	151132.8
050604095	153620.5	153642.3
050604094	150235.6	150248.4
050604093	150902.5	150905.4
062404408	103932.2	103938.5

Table 7: Material C Filter Weights

Run #9 - Blank 3 (Run Time = 1.45 hours)

MOUDI Position	Filter Number	Initial Weight (µg)	Final Weight (µg)
1	051004114	164495.8	164501.9
2	051004113	161922.7	161924.4
3	051004112	161966.6	161968.3
4	051004111	159358.6	159364.0
5	051004110	161622.3	161625.6
6	051004109	157109.6	157119.5
7	051004108	161641.9	161654.3
8	051004107	158933.3	158942.7
9	051004106	162497.1	162506.3
10	051004105	159164.8	159151.7
11	051004104	162781.7	162784.5
12	062404409	101906.9	101909.5

Run #11 - Material C (Run Time = 2.92 hours)

MOUDI Position	Filter Number	Initial Weight (µg)	Final Weight (µg)
1	051004136	157408.4	157416.9
2	051004135	160911.5	160922.5
3	051004134	166122.4	166144.7
4	051004133	166111.3	166144.6
5	051004132	155644.6	155671.5
6	051004131	163973.8	164006.7
7	051004130	162507.6	162511.3
8	051004129	158707.5	158725.6
9	051004128	157964.2	157977.4
10	051004127	154899.1	154901.2
11	051004126	158015.5	158016.1
12	062404411	100695.1	100696.9

Run #12 - Material C (Run Time = 2.57 hours)

Filter Number	Initial Weight (µg)	Final Weight (µg)
051004147	162827.7	162839.2
051004146	166533.0	166538.3
051004145	160962.4	160973.3
051004144	156690.8	156720.5
051004143	163865.8	163895.8
051004142	164038.7	164070.8
051004141	164927.3	164954.1
051004140	164987.8	165001.9
051004139	164710.2	164727.7
051004138	158630.5	158633.5
051004137	163369.9	163371.7
062404412	98379.0	98384.1

Run #13 - Material C (Run Time = 2.72 hours)

Filter Number	Initial Weight (µg)	Final Weight (µg)
051304158	158988.7	158998.6
051304157	162628.2	162632.5
051304156	167470.9	167487.1
051304155	166961.7	166994.5
051304154	171869.9	171895.6
051304153	162624.3	162649.3
051304152	162907.4	162924.5
051304151	163645.1	163657.4
051004150	165869.7	165871.4
051004149	153986.7	153991.4
051004148	158177.8	158179.0
062404413	95798.9	95801.8

Appendix D: Chemical Analysis for Cu & Fe

Table 8: Copper Mass

	Run #1 - Blank 1	Run #2 - Material A	Run #3 - Material A	Run #4 - Material A
MOUDI Position	Copper (µg)	Copper (µg)	Copper (µg)	Copper (µg)
1	0.76	1.04	0.91	2.85
2	0.59	2.03	2.02	1.85
3	0.48	4.43	6.67	6.83
4	0.53	8.58	13.69	14.80
5	0.52	8.21	4.74	3.54
6	0.56	7.75	9.61	7.10
7	0.50	2.87	5.33	0.84
8	0.34	2.43	2.57	3.61
9	0.64	2.18	2.33	1.97
10	0.51	1.09	1.57	2.79
11	0.64	0.48	0.69	0.25
12	0.80	0.60	0.83	0.58
	Run#5 - Blank 2	**Run#6 - Material B**	**Run#7 - Material B**	**Run#8 - Material B**
MOUDI Position	Copper (µg)	Copper (µg)	Copper (µg)	Copper (µg)
1	0.15	3.64	2.45	4.50
2	0.2	1.76	3.41	3.03
3	0.16	6.36	14.61	10.67
4	0.22	14.71	13.31	16.38
5	0.33	7.13	9.62	8.12
6	0.19	3.55	6.10	3.17
7	0.15	1.95	3.84	3.55
8	0.39	1.55	2.31	1.93
9	0.19	1.12	1.04	1.40
10	0.25	0.47	0.81	1.14
11	0.06	0.10	0.66	0.61
12	0.43	0.35	1.10	1.03
	Run#9 - Blank 3	**Run#11 - Material C**	**Run#12 - Material C**	**Run#13 - Material C**
MOUDI Position	Copper (µg)	Copper (µg)	Copper (µg)	Copper (µg)
1	0.44	0.60	2.58	0.69
2	0.37	0.59	0.59	0.65
3	0.34	1.10	0.93	1.14
4	0.35	1.23	0.94	1.40
5	0.54	0.92	1.43	2.01
6	0.35	0.78	2.57	1.36
7	0.64	1.03	1.12	1.26
8	0.47	0.65	0.94	1.02
9	0.39	0.64	0.42	0.68
10	0.52	0.58	0.64	0.38
11	0.27	0.48	0.42	0.74
12	0.41	0.87	0.38	0.72

Table 9: Iron Mass

	Run #1 - Blank 1	Run #2 - Material A	Run #3 - Material A	Run #4 - Material A
MOUDI Position	Iron (µg)	Iron (µg)	Iron (µg)	Iron (µg)
1	7.71	2.53	3.36	6.46
2	5.72	9.59	9.37	5.35
3	6.67	7.90	14.17	12.63
4	5.23	14.09	22.05	30.51
5	6.96	13.63	8.49	11.46
6	3.49	13.12	18.80	16.39
7	1.23	7.64	15.61	3.11
8	0.96	4.17	7.62	10.07
9	2.03	5.18	5.31	10.89
10	1.22	2.82	9.79	8.37
11	2.63	2.50	4.70	0.79
12	3.91	2.44	3.16	2.82

	Run#5 - Blank 2	Run#6 - Material B	Run#7 - Material B	Run#8 - Material B
MOUDI Position	Iron (µg)	Iron (µg)	Iron (µg)	Iron (µg)
1	3.35	21.78	15.37	25.35
2	5.45	17.12	19.52	17.07
3	9.02	43.41	67.92	52.10
4	3.39	100.10	69.90	86.80
5	6.58	57.20	56.40	45.41
6	4.19	32.16	38.04	22.04
7	5.75	17.66	24.32	24.55
8	6.50	16.09	14.40	12.52
9	11.07	12.60	6.75	13.33
10	6.72	3.91	6.53	15.20
11	3.04	2.89	7.11	2.92
12	5.96	4.32	6.29	6.66

	Run#9 - Blank 3	Run#11 - Material C	Run#12 - Material C	Run#13 - Material C
MOUDI Position	Iron (µg)	Iron (µg)	Iron (µg)	Iron (µg)
1	1.89	4.36	5.46	3.33
2	2.71	4.71	12.08	4.20
3	2.04	6.20	3.44	4.72
4	2.70	5.45	2.98	3.98
5	3.89	5.05	3.13	4.18
6	3.48	6.09	5.16	5.95
7	2.06	10.92	6.39	4.27
8	6.95	6.21	3.68	20.57
9	3.85	5.32	3.02	4.08
10	2.76	6.88	2.49	3.38
11	3.26	3.27	3.58	8.47
12	3.80	6.31	4.04	9.31

Appendix E: Characteristic Values of the Cu-Based Particle Size Distribution for Use in the Air Deposition Model

The air deposition study conducted by AER utilizes two different resolution models. One is a fine grid model used for the airshed above Castro Valley, while the other is a coarse grid model used for entire airshed of the San Francisco Bay area. Although both models utilize the copper-based aerodynamic particle size distribution information as an input parameter, each model requires slightly different characteristic information about the Cu-based PSD.

The fine grid model uses the actual size distribution itself to examine uncertainty in the model output. For this model, the Cu-based PSD needs to be characterized by a central value (i.e., the mass median aerodynamic diameter which is also referred to as d_{50}) and upper and lower characteristic values. For AER's fine grid model, the upper and lower characteristic values were selected to be the upper and lower quartile values, or d_{75} and d_{25}. AER's coarse grid model uses the central value only as an input parameter, but uncertainty in the model output is tested by examining what effect the uncertainty in the d_{50} value has on the result.

Cumulative aerodynamic particle size distributions based on total mass, copper analysis, and iron analysis and their associated uncertainties based on error propagation are summarized in Table 10 and also shown in Figure E-1. To obtain the values needed for the fine grid model, the 25%, 50% and 75% characteristic values for the Cu-based PSD were obtained by simple interpolation using the mean values shown for each size bin. The results are:

Fine model
central value = d_{50} = 3.5 µm
lower value = d_{25} = 1.5 µm
upper value = d_{75} = 5.6 µm

To obtain the values needed for the coarse grid model, the upper/lower limits of the central value were obtained by simple interpolation using the upper/lower uncertainty values for all size bins as if they were independent particle size distributions. The results are:

Coarse model
central value = d_{50} = 3.5 µm
lower uncertainty limit of central value = 3.1 µm
upper uncertainty limit of central value = 4.0 µm

Table 10. Cumulative percent particle size distributions

Particle Size Cutoff, µm	% of total particulate mass	% of total particulate copper mass	% of total particulate iron mass
all particles	100.00 ± 5.39	100.00 ± 8.47	100.00 ± 19.21
< 18	93.80 ± 5.20	94.76 ± 7.91	95.70 ± 18.56
< 10	88.65 ± 5.02	91.18 ± 7.73	91.15 ± 17.58
< 5.6	70.88 ± 4.46	74.66 ± 6.72	75.79 ± 15.49
< 3.2	44.48 ± 3.45	46.23 ± 5.00	43.64 ± 12.52
< 1.8	24.74 ± 2.87	31.97 ± 3.99	29.09 ± 11.60
< 1	12.11 ± 2.37	15.76 ± 2.87	15.97 ± 10.97
< 0.56	6.84 ± 1.76	9.42 ± 1.80	5.49 ± 10.10
< 0.32	2.62 ± 1.60	4.62 ± 1.55	3.38 ± 6.80
< 0.18	0.77 ± 1.25	2.01 ± 1.39	2.55 ± 4.63
< 0.1	0.50 ± 0.73	0.25 ± 1.02	0.49 ± 3.06
< 0.056	0.50 ± 0.42	0.05 ± 0.61	0.00 ± 2.05

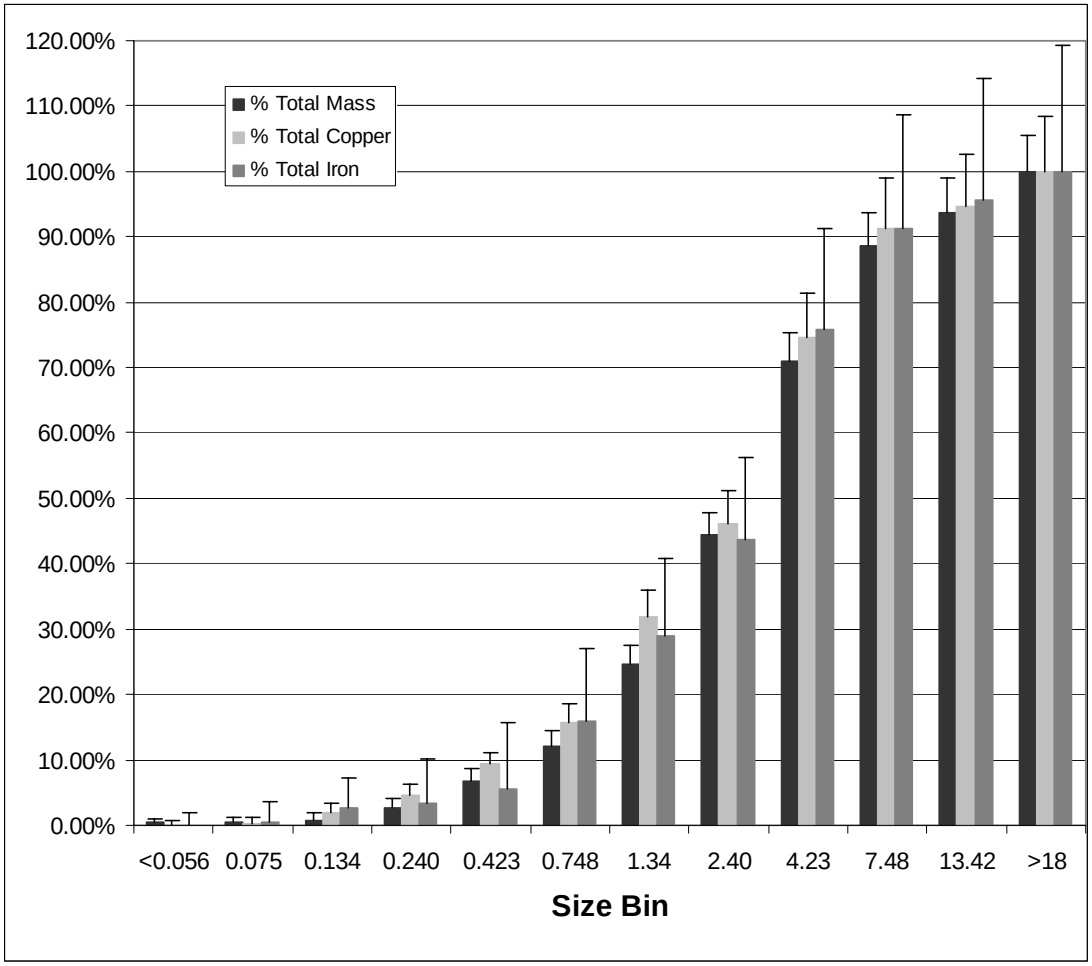

Figure E-1. Cumulative percent particle size distributions